Xiang-Yu Yan, De-Bin Yang, Wen-Liang Xu, Hao-Tian Yang, Mao-Song Mu, An-Qi Wang, Yi-Kang Quan, and Le-Ran Hao, 2022, Modification of the lithospheric mantle induced by recycled crustal components: Insights from Early Cretaceous appinites from the Liaodong Peninsula, NE China: GSA Bulletin, https://doi.org/10.1130/B36352.1.

Supplemental Material

Figure S1. Representative field photographs and photomicrographs.

Text. Details of the analytical methods.

Figure S2. Harker variation diagrams of selected major- and trace-element contents.

Figure S3. The selected trace element and isotopic geochemical diagrams.

Table S1. LA-ICP-MS U-Pb isotopic data for zircons in Early Cretaceous appinites.

Table S2. Major and trace element data for the Early Cretaceous appinites.

Table S3. Whole-rock Sr–Nd–Pb isotopic data for Early Cretaceous appinites.

Table S4. In situ zircon Hf–O isotopic data for Early Cretaceous appinites.

Table S5. Major and trace element data of plagioclase.

Table S6. In situ Pb isotopes of plagioclase.

Summary of cited references in main text Figures 1, 2, 4, 5, and 6.

Figure S1. Representative field photographs and photomicrographs.

Figure S1. Representative field photographs and photomicrographs in the studied appinites. Amp—Amphibole; Bi—Biotite; Cpx—Clinopyroxene; Pl—Plagioclase. Typical reaction relationships between clinopyroxene and amphibole in the appinites.

Text. Details of the analytical methods

1. Zircon LA-ICP-MS U-Pb dating

Zircon grains were separated from all appinites (16L03-1, 16L05-1, 19L11-1, 16L13-1, 17L02-1, 17L02-1-O, 17L06-1, 17L06-9 and DD17-1-O), using conventional density and magnetic techniques at the laboratory of Langfang Regional Geological Survey Institute, Hebei Province, China. Subsequently, zircon grains were individually selected by hand-picking and carefully mounted in epoxy resin, and polished to expose the grain center. Zircon CL images were obtained at the Wuhan SampleSolution Analytical Technology Co., Ltd., Wuhan, China, using an Analytical Scanning Electron Microscope (JSM−IT100) connected to a GATAN MINICL system. The imaging condition was 10.0−13.0 kV voltage of electric field and 80−85 μA current of tungsten filament.

Zircon U-Pb dating and trace element analysis of zircon simultaneously measured by LA-ICP-MS at the Key Laboratory of Mineral Resources Evaluation in Northeast Asia, Ministry of Natural Resources, Jilin University, Changchun, China, using a GeolasPro LA system coupled with an Agilent 7700e ICP-MS instrument, and data reduction are the same as description by Zong et al. (2017). Laser sampling was performed using a GeolasPro laser ablation system that consists of a COMPexPro 102 ArF excimer laser (wavelength of 193 nm and maximum energy of 200 mJ) and a MicroLas optical system. An Agilent 7700e ICP-MS instrument was used to acquire ion-signal intensities. The spot size and frequency of the laser were set to 32μm or 24μm and 5 Hz or 4 Hz, respectively, in this study. Zircon 91500 and glass NIST610 were used as external standards for U-Pb dating and trace element calibration, respectively. Each analysis incorporated a background acquisition of ~20–30 s followed by 50 s of data acquisition from the sample. An Excel-based software ICPMSDataCal was used to perform off-line selection and integration of background and analyzed signals, time-drift correction and quantitative calibration for trace element analysis and U-Pb dating (Liu et al., 2008; Liu et al., 2010). Concordia diagrams and weighted mean calculations were made using Isoplot/Ex_ver3 (Ludwig, 2003).

2. Whole-rock Major and trace element analyses

Major element analyses of whole rock were conducted on XRF (Primus II, Rigaku, Japan) at the Wuhan SampleSolution Analytical Technology Co., Ltd., Wuhan, China. The analytical precision (relative standard deviation, RSD) and accuracy (relative error, RE) are both better than 4% for the major element concentrations measured in this study, and further details of the analytical procedures used are given in Ma et al. (2012). Trace element analysis of whole rock were conducted on Agilent 7700e ICP-MS at the Wuhan SampleSolution Analytical Technology Co., Ltd., Wuhan, China. Sample digestion procedures and the resulting analytical precision and accuracy are reported in Liu et al. (2008).

3. Whole-rock Sr-Nd-Pb isotopes composition

Whole-rock Sr-Nd-Pb isotope analyses were performed on a Neptune Plus MC-ICP-MS (Thermo Fisher Scientific, Dreieich, Germany) at the Wuhan SampleSolution Analytical Technology Co., Ltd, Hubei, China, following the methods of Gao et al. (2004). For Sr, Nd isotope measurements, ~100 mg sample powders were dissolved in Teflon bombs using HF-HNO_3 mixtures under high temperature. After centrifugation, columns of AG50W-X8 and LN resins were used sequentially for separation and purification of REEs and finally for separation of Nd and Sm by HCl eluants using

published procedures. For Pb isotopes, samples of ~100 mg were dissolved in Teflon bombs using HF-HNO_3 mixtures. The supernatant solution was loaded into an ion-exchange column packed with AG 1-X8 anionic resin to elute Pb using 6 M HCl. Analyses of NBS-981 standard yielded external precisions of 0.03% (2σ) for $^{208}Pb/^{204}Pb$, $^{207}Pb/^{204}Pb$ and $^{206}Pb/^{204}Pb$. Measured values for NBS-981 Pb isotopes standard were 36.726 for $^{208}Pb/^{204}Pb$, 15.500 for $^{207}Pb/^{204}Pb$ and 16.941 for $^{206}Pb/^{204}Pb$.

4. Zircon Hf isotopes

Experiments of in situ Hf isotope ratio analysis were conducted using a Neptune Plus MC-ICP-MS (Thermo Fisher Scientific, Germany) in combination with a Geolas HD excimer ArF laser ablation system (Coherent, Göttingen, Germany) that was hosted at the State Key Laboratory of Geological Processes and Mineral Resources, China University of Geosciences, Wuhan, China. A "wire" signal smoothing device is included in this laser ablation system, by which smooth signals are produced even at very low laser repetition rates down to 1 Hz (Hu et al., 2012). Helium was used as the carrier gas within the ablation cell and was merged with argon (makeup gas) after the ablation cell. Small amounts of nitrogen were added to the argon makeup gas flow for the improvement of sensitivity of Hf isotopes (Hu et al., 2008). Compared to the standard arrangement, the addition of nitrogen in combination with the use of the newly designed X skimmer cone and Jet sample cone in Neptune Plus improved the signal intensity of Hf, Yb and Lu by a factor of 5.3, 4.0 and 2.4, respectively. All data were acquired on zircon in single spot ablation mode at a spot size of 44 μm. The energy density of laser ablation that was used in this study was ~7.0 J cm-2. Each measurement consisted of 20 s of acquisition of the background signal followed by 50 s of ablation signal acquisition. Detailed operating conditions for the laser ablation system and the MC-ICP-MS instrument and analytical method are the same as description by Hu et al. (2012). Off-line selection and integration of analyte signals, and mass bias calibrations were performed using ICPMSDataCal (Liu et al., 2010).

5. Zircon O isotopes

Zircon oxygen isotopic data were measured by a Cameca IMS 1280 ion microprobe at the State Key Laboratory of Isotope Geochemistry, Guangzhou Institute of Geochemistry, Chinese Academy of Sciences, Guangzhou, China. The target was pre-sputtered for 35 s using a 20 μm square raster to remove the Au coating, with analysis using a 50 eV energy slit and 5 V shifts below the maximum transmission. We used the Penglai zircon standard as external standardization and three other reference zircon samples (91500, Qinghu, and Temora 2) were used as unknowns to check the accuracy and precision of the analyses. A value of $\delta^{18}O = 5.31‰ \pm 0.10‰$ (2SD) was obtained for the Penglai zircon analyzed in this study (Li et al., 2010; Yang et al., 2018).

6. In situ Pb isotopes of plagioclases

Pb isotope ratios of feldspars were measured by a Neptune Plus MC-ICP-MS (Thermo Fisher Scientific, Bremen, Germany) using a combination of Faraday cups and ion counters (FC-IC) in combination with a Geolas HD excimer ArF laser ablation system (Coherent, Göttingen, Germany) at the State Key Laboratory of Geological Processes and Mineral Resources, China University of Geosciences, Wuhan, China. In the FC-IC array, ^{208}Pb, ^{207}Pb and ^{206}Pb were measured using Faraday cups, and ^{204}Pb and ^{202}Hg were measured using three ICs mounted on the low mass Faraday cups. In the laser ablation system, helium was used as the carrier gas for the ablation cell and was mixed with

argon (makeup gas) after the ablation cell. For a single laser spot ablation, the spot diameter ranged from 90 to 160 μm dependent on Pb signal intensity. The pulse frequency was from 8 to 15 Hz, but the laser fluence was kept constant at ~10 J/cm^2. A new signal smoothing and mercury-removing device (Hu et al., 2015) was used downstream from the sample cell to eliminate the short-term variation of the signal and reduce the background of Hg in the carrier gas.

7. REFERENCES CITED

Gao, S., Rudnick, R.L., Yuan, H.L., Liu, X.M., Liu, Y.S., Xu, W.L., Ling, W.L., Ayers, J., Wang, X.C., and Wang, Q.H., 2004, Recycling lower continental crust in the North China craton: Nature, v. 432, p. 892–897, https://doi.org/10.1038/nature03162.

Hu, Z.C., Gao, S., Liu, Y.S., Hu, S.H., Chen, H.H., and Yuan, H.L., 2008, Signal Enhancement in Laser Ablation ICP-MS by Addition of Nitrogen in the Central Channel Gas: Journal of Analytical Atomic Spectrometry, v. 23, p. 1093–1101, https://doi.org/10.1039/b804760j.

Hu, Z.C., Liu, Y.S., Gao, S., Liu, W.G., Yang, L., Zhang, W., Tong, X.R., Lin, L., Zong, K.Q., Li, M., Chen, H.H., and Zhou, L., 2012, Improved in situ Hf isotope ratio analysis of zircon using newly designed X skimmer cone and jet sample cone in combination with the addition of nitrogen by laser ablation multiple collector ICP-MS: Journal of Analytical Atomic Spectrometry, v. 27, p. 1391–1399, https://doi.org/10.1039/c2ja30078h.

Hu, Z.C., Zhang, W., Liu, Y.S., Gao, S., Li, M., Zong, K.Q., Chen, H.H., and Hu, S.H., 2015, "Wave" signal smoothing and mercury removing device for laser ablation quadrupole and multiple collector ICP-MS analysis: application to lead isotope analysis: Analytical Chemistry, v. 87, p. 1152–1157, https://doi.org/10.1021/ac503749k.

Li, X.H., Long, W.G., Li, Q.L., Liu, Y., Zheng, Y.F., Yang, Y.H., Chamberlain, K.R., Wan, D.F., Guo, C.H., Wang, X.C., and Tao, H., 2010, Penglai zircon megacrysts: A potential new working reference material for microbeam determination of Hf-O isotopes and U-Pb age: Geostandards and Geoanalytical Research, v. 34, p. 117–134, https://doi.org/10.1111/j.1751-908X.2010.00036.x.

Liu, Y.S., Zong, K.Q., Kelemen, P.B., and Gao, S., 2008, Geochemistry and magmatic history of eclogites and ultramafic rocks from the Chinese continental scientific drill hole: subduction and ultrahigh-pressure metamorphism of lower crustal cumulates: Chemical Geology, v. 247, p. 133–153, https://doi.org/10.1016/j.chemgeo.2007.10.016.

Liu, Y.S., Gao, S., Hu, Z.C., Gao, C.G., Zong, K.Q., and Wang, D.B., 2010, Continental and oceanic crust recycling-induced melt-peridotite interactions in the Trans-North China Orogen: U-Pb dating, Hf isotopes and trace elements in zircons of mantle xenoliths: Journal of Petrology, v. 51, p. 537–571, https://doi.org/10.1093/petrology/egp082.

Ludwig, K.R., 2003, User's manual for Isoplot 3.00: a geochronological toolkit for microsoft excel: Berkeley Geochronology Centre Special Publication 4, 74 p.

Ma, Q., Zheng, J.P., Griffin, W.L., Zhang, M., Tang, H.Y., Su, Y.P., and Ping, X.Q., 2012, Triassic "adakitic" rocks in an extensional setting (North China): melts from the cratonic lower crust: Lithos, v. 149, p. 159–173, https://doi.org/10.1016/j.lithos.2012.04.017.

Yang, Q., Xia, X.P., Zhang, W.F., Zhang, Y.Q., Xiong, B.Q., Xu, Y.G., Wang, Q., and Wei, G.J., 2018, An evaluation of precision and accuracy of SIMS oxygen isotope analysis: Solid Earth Science, v. 3, p. 81–86, https://doi.org/10.1016/j.sesci.2018.05.001.

Zong, K.Q., Klemd, R., Yuan, Y., He, Z.Y., Guo, J.L., Shi, X.L., Liu, Y.S., Hu, Z.C., and Zhang, Z.M., 2017, The assembly of Rodinia: the correlation of early Neoproterozoic (ca. 900 Ma) high-grade metamorphism and continental arc formation in the southern Beishan Orogen, southern Central Asian Orogenic Belt (CAOB): Precambrian Research, v. 290, p. 32–48, https://doi.org/10.1016/j.precamres.2016.12.010.

Figure S2. Harker variation diagrams of selected major- and trace-element contents.

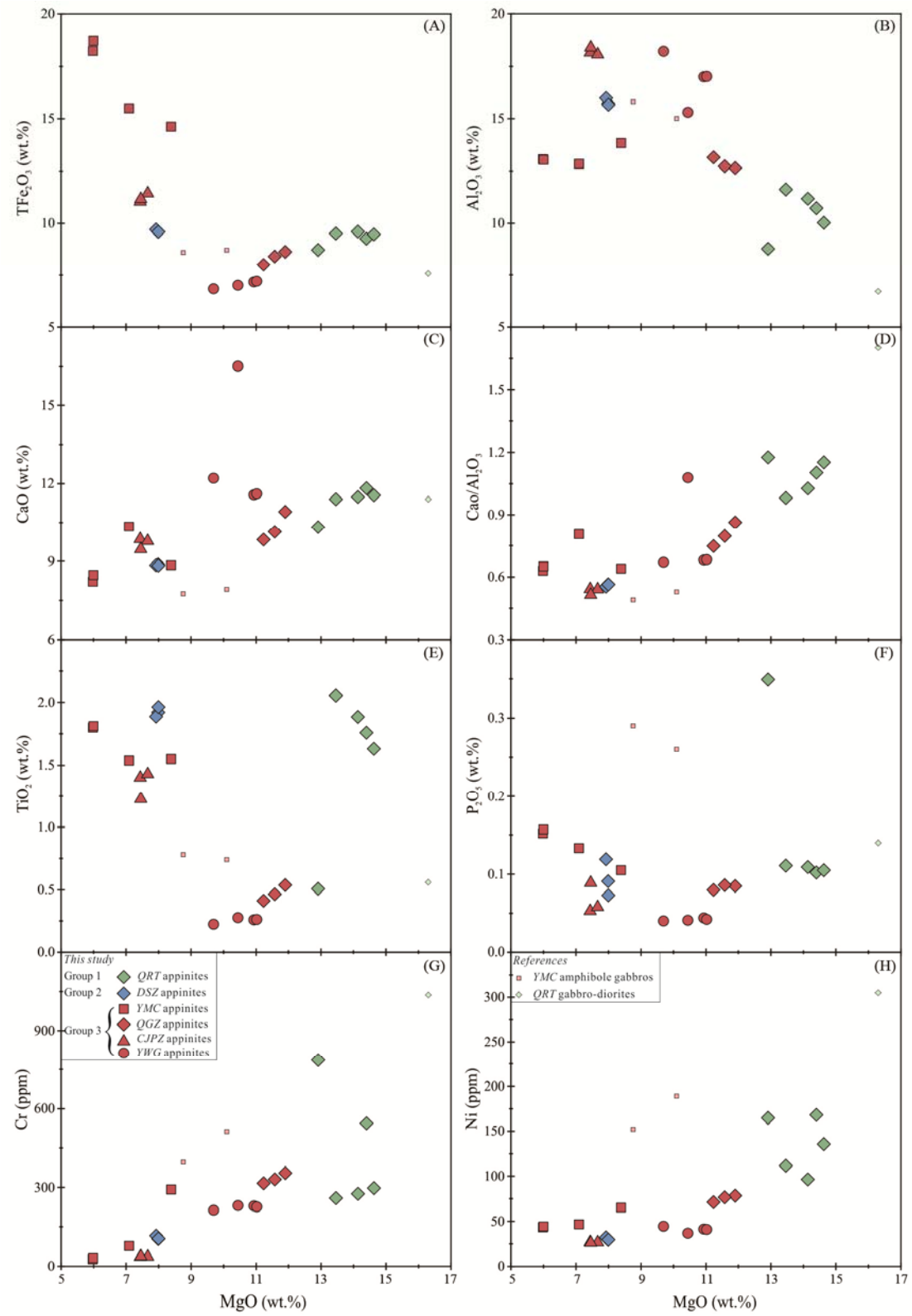

Figure S2. Harker variation diagrams of selected major- and trace-element contents versus MgO. (A) TFe_2O_3, (B) Al_2O_3, (C) CaO, (D) Cao/Al_2O_3, (E) TiO_2, (F) P_2O_5, (G) Cr, (H) Ni. The specific data sources for studied appinites, *YMC* amphibole gabbros and *QRT* gabbro-diorites are from Table S2 and the summary of cited references.

Figure S3. The selected trace element and isotopic geochemical diagrams.

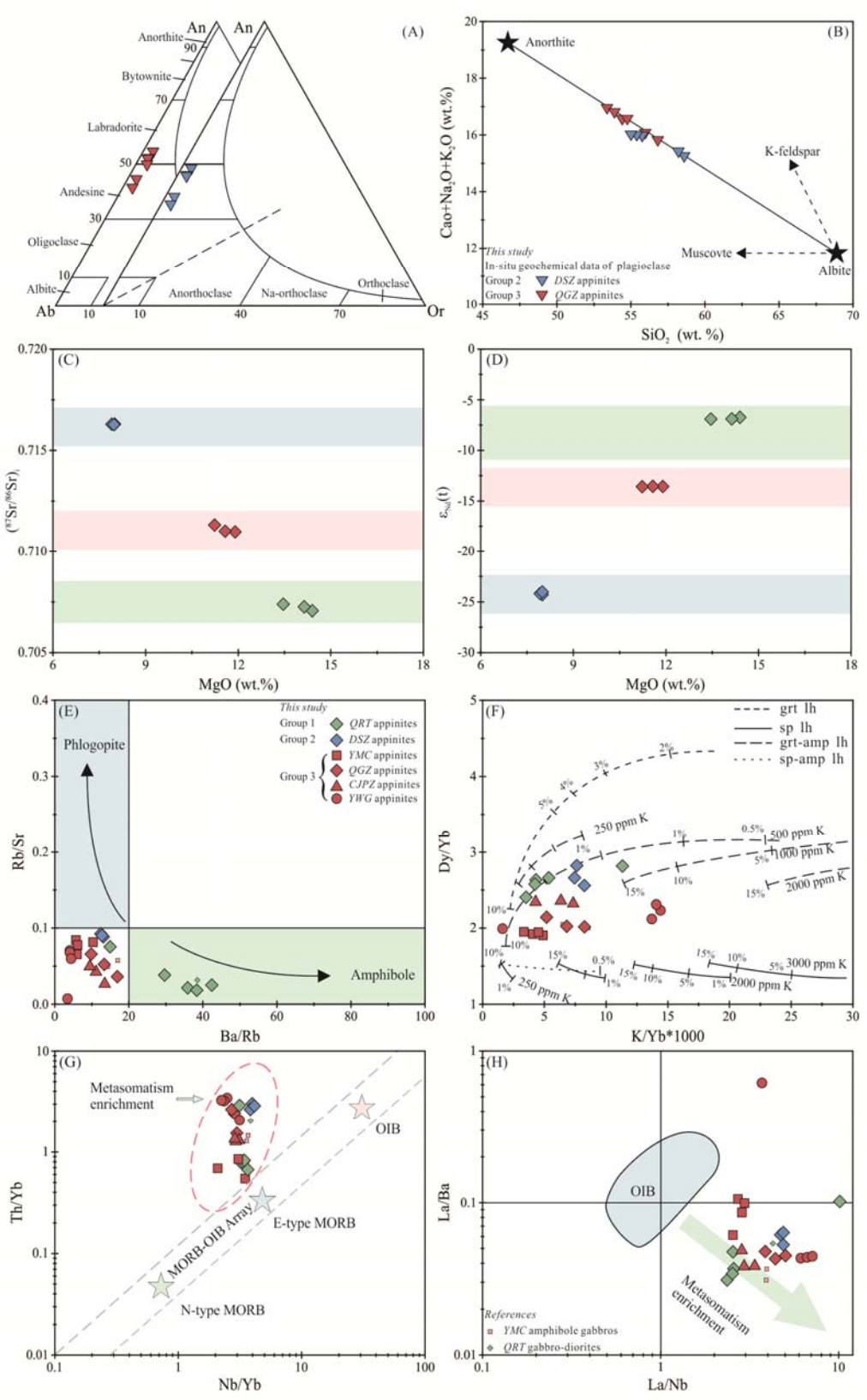

Figure S3. A classification diagram of plagioclase (A), and $CaO + Na_2O + K_2O$ versus SiO_2 (B) diagram for plagioclase (Williamson et al., 2016; Zarasvandi et al., 2019). Discrimination diagrams of (C) $(^{87}Sr/^{86}Sr)_i$ versus MgO, (D) $\varepsilon_{Nd}(t)$ versus MgO. Plots of (E) Rb/Sr versus Ba/Rb (Furman and

Graham, 1999), (F) Dy/Yb versus K/(Yb*1000) (Duggen et al., 2005), (G) Th/Yb versus Nb/Yb (Pearce, 2008), and (H) La/Ba versus La/Nb (Liu et al., 2020). An—anorthite; Ab—albite; Or—Orthoclase. Melting curves for garnet lherzolite (grt lh), spinel lherzolite (sp lh), garnet-facies amphibole lherzolite (grt-amp lh) and spinel-facies amphibole lherzolite (sp-amp lh) are taken from Duggen et al. (2005). The compositions of OIB and MORB are from Sun and McDonough (1989). The specific data sources for studied appinites, *YMC* amphibole gabbros and *QRT* gabbro-diorites are from Tables S2, S3, S5, and the summary of cited references.

REFERENCES CITED

Duggen, S., Hoernle, K., Van, D.B.P., and Garbe-Schönberg, D., 2005, Post-collisional transition from subduction- to intraplate-type magmatism in the westernmost Mediterranean: evidence for continental-edge delamination of subcontinental lithosphere: Journal of Petrology, v. 46, p. 1155–1201, https://doi.org/10.1093/petrology/egi013.

Furman, T., and Graham, D., 1999, Erosion of lithospheric mantle beneath the East African Rift system: geochemical evidence from the Kivu volcanic province: Developments in Geotectonics, v. 24, p. 237–262, https://doi.org/10.1016/S0419-0254(99)80014-7.

Liu, Y., Wei, J.H., Zhang, D.H., Chen, J.J., and Zhang, X.M., 2020, Early Cretaceous Wulong intermediate-mafic dike swarms in the Liaodong Peninsula: Implications for rapid lithospheric delamination of the North China Craton: Lithos, v. 362–363, p. 105473, https://doi.org/10.1016/j.lithos.2020.105473.

Pearce, J.A., 2008, Geochemical fingerprinting of oceanic basalts with applications to ophiolite classification and the search for Archean oceanic crust: Lithos, v. 100, p. 14–48, https://doi.org/10.1016/j.lithos.2007.06.016.

Sun, S.S., and McDonough, W.F., 1989, Chemical and isotopic systematics of oceanic basalts: implications for mantle composition and processes: Geological Society of London, Special Publications, v. 42, p. 313–345, https://doi.org/10.1144/GSL.SP.1989.042.01.19.

Williamson, B.J., Herrington, R.J., and Morris, A., 2016, Porphyry copper enrichment linked to excess aluminium in plagioclase: Nature Geoscience, v. 9, p. 237–241, https://doi.org/10.1038/ngeo2651.

Zarasvandi, A., Heidari, M., Raith, J., Rezaei, M., and Saki, A., 2019, Geochemical characteristics of collisional and pre-collisional porphyry copper systems in Kerman Cenozoic Magmatic Arc, Iran: Using plagioclase, biotite and amphibole chemistry: Lithos, v. 326–327, p. 279–297, https://doi.org/10.1016/j.lithos.2018.12.029.

Table S1. LA-ICP-MS U-Pb isotopic data for zircons in Early Cretaceous appinites

Spot no.	Th	U	Th/U	$^{207}Pb/^{206}Pb$		$^{207}Pb/^{235}U$		$^{206}Pb/^{238}U$		$^{207}Pb/^{206}Pb$		$^{207}Pb/^{235}U$		$^{206}Pb/^{238}U$	
	(ppm)	(ppm)		Ratio	1σ	Ratio	1σ	Ratio	1σ	Age(Ma)	1σ	Age(Ma)	1σ	Age(Ma)	1σ
16L03-1-01	301	408	0.74	0.04981	0.00191	0.12940	0.00494	0.01889	0.00020	186	69	124	4	121	1
16L03-1-02	179	251	0.71	0.04904	0.00233	0.12584	0.00564	0.01863	0.00022	150	82	120	5	119	1
16L03-1-03	141	331	0.43	0.05280	0.00251	0.13557	0.00635	0.01885	0.00023	320	84	129	6	120	1
16L03-1-04	156	261	0.60	0.05148	0.00250	0.13317	0.00659	0.01882	0.00023	262	92	127	6	120	1
16L03-1-05	158	459	0.34	0.04681	0.00199	0.11928	0.00478	0.01871	0.00021	39	66	114	4	119	1
16L03-1-06	120	113	1.06	0.04442	0.00437	0.12441	0.01199	0.01988	0.00049	-49	161	119	11	127	3
16L03-1-07	140	256	0.54	0.04986	0.00689	0.13209	0.01910	0.01943	0.00029	189	277	126	17	124	2
16L03-1-08	131	133	0.98	0.04775	0.00356	0.12337	0.00782	0.01936	0.00033	87	109	118	7	124	2
16L03-1-09	68	113	0.60	0.05786	0.00480	0.14030	0.00931	0.01853	0.00037	525	111	133	8	118	2
16L03-1-10	137	201	0.68	0.04568	0.00313	0.11527	0.00715	0.01863	0.00027	-19	106	111	7	119	2
16L03-1-11	161	172	0.94	0.04995	0.00280	0.12774	0.00671	0.01892	0.00026	192	96	122	6	121	2
16L03-1-12	163	162	1.01	0.05381	0.00326	0.13384	0.00720	0.01835	0.00026	363	96	128	6	117	2
16L03-1-13	157	239	0.66	0.05058	0.00309	0.12925	0.00699	0.01899	0.00026	222	100	123	6	121	2
16L03-1-14	125	186	0.67	0.04843	0.00277	0.12304	0.00667	0.01884	0.00028	120	95	118	6	120	2
16L03-1-15	159	440	0.36	0.05169	0.00464	0.13500	0.01200	0.01889	0.00024	272	178	129	11	121	2
16L03-1-16	389	926	0.42	0.04726	0.00178	0.12377	0.00478	0.01897	0.00019	62	67	118	4	121	1
16L03-1-17	104	98	1.06	0.05789	0.00476	0.14699	0.01043	0.01925	0.00038	526	122	139	9	123	2
16L03-1-18	121	109	1.11	0.05526	0.00466	0.14276	0.01102	0.01946	0.00035	423	141	136	10	124	2
16L05-1-01	1506	824	1.83	0.05489	0.00132	0.15079	0.00398	0.01979	0.00022	408	39	143	4	126	1
16L05-1-02	175	159	1.10	0.05711	0.00267	0.15316	0.00681	0.01946	0.00030	496	70	145	6	124	2
16L05-1-03	570	373	1.53	0.04792	0.00130	0.13015	0.00363	0.01958	0.00028	95	40	124	3	125	2
16L05-1-04	354	294	1.20	0.05043	0.00187	0.13807	0.00538	0.01970	0.00036	215	57	131	5	126	2
16L05-1-05	1284	709	1.81	0.04904	0.00113	0.13325	0.00289	0.01960	0.00032	150	24	127	3	125	2

16L05-1-06	343	270	1.27	0.04935	0.00199	0.13313	0.00539	0.01950	0.00040	165	57	127	5	124	3
16L05-1-07	813	428	1.90	0.05375	0.00253	0.14668	0.00589	0.01970	0.00045	361	51	139	5	126	3
16L05-1-08	116	100	1.16	0.04914	0.00375	0.13235	0.01089	0.01955	0.00058	155	130	126	10	125	4
16L05-1-09	322	290	1.11	0.04978	0.00203	0.13521	0.00576	0.01972	0.00044	185	59	129	5	126	3
16L05-1-10	413	306	1.35	0.04701	0.00146	0.12828	0.00440	0.01967	0.00029	50	49	123	4	126	2
16L05-1-11	393	498	0.79	0.04754	0.00121	0.13054	0.00379	0.01982	0.00032	77	39	125	3	127	2
16L05-1-12	733	464	1.58	0.05075	0.00246	0.13614	0.00634	0.01944	0.00037	230	72	130	6	124	2
16L05-1-13	581	390	1.49	0.04739	0.00132	0.12784	0.00377	0.01948	0.00025	69	45	122	3	124	2
16L05-1-14	179	178	1.01	0.04768	0.00602	0.12882	0.01575	0.01960	0.00062	83	254	123	14	125	4
16L05-1-15	281	258	1.09	0.04948	0.00258	0.13291	0.00665	0.01955	0.00032	171	86	127	6	125	2
16L05-1-16	409	378	1.08	0.04757	0.00152	0.12682	0.00462	0.01928	0.00049	78	43	121	4	123	3
16L05-1-17	1257	651	1.93	0.04979	0.00242	0.13612	0.00651	0.01978	0.00022	185	90	130	6	126	1
16L05-1-18	561	390	1.44	0.04605	0.00306	0.12273	0.00770	0.01933	0.00042	-	146	118	7	123	3
16L05-1-19	175	193	0.91	0.04605	0.00355	0.12419	0.00931	0.01956	0.00035	-	171	119	8	125	2
16L05-1-20	1411	812	1.74	0.04981	0.00303	0.13444	0.00832	0.01950	0.00028	186	115	128	7	125	2
19L11-1-01	93	74	1.26	0.06927	0.00749	0.16580	0.01363	0.01884	0.00079	907	102	156	12	120	5
19L11-1-02	1111	868	1.28	0.05021	0.00213	0.13037	0.00559	0.01883	0.00026	205	74	124	5	120	2
19L11-1-03	448	224	2.00	0.04733	0.00276	0.12101	0.00705	0.01888	0.00038	66	91	116	6	121	2
19L11-1-04	86	85	1.01	0.05000	0.00610	0.12755	0.01524	0.01850	0.00046	195	266	122	14	118	3
19L11-1-05	190	149	1.28	0.05761	0.00426	0.14040	0.00917	0.01889	0.00041	515	105	133	8	121	3
19L11-1-06	137	179	0.77	0.05387	0.00331	0.13629	0.00803	0.01876	0.00035	366	99	130	7	120	2
19L11-1-07	89	80	1.11	0.06269	0.00665	0.15107	0.01263	0.01881	0.00057	698	127	143	11	120	4
19L11-1-08	66	90	0.73	0.07087	0.01432	0.16503	0.02570	0.01901	0.00087	954	249	155	22	121	5
19L11-1-09	45	47	0.97	0.09444	0.01563	0.24042	0.03788	0.01846	0.00093	1517	336	219	31	118	6
19L11-1-10	170	124	1.36	0.05460	0.00446	0.13997	0.01055	0.01892	0.00045	396	126	133	9	121	3
19L11-1-11	108	128	0.85	0.06942	0.00741	0.16679	0.01441	0.01896	0.00066	911	121	157	13	121	4
19L11-1-12	125	91	1.37	0.06304	0.00523	0.15751	0.01109	0.01874	0.00054	710	100	149	10	120	3
19L11-1-13	52	61	0.85	0.10205	0.00907	0.23284	0.01771	0.01886	0.00058	1662	95	213	15	120	4
19L11-1-14	976	715	1.36	0.05058	0.00198	0.13159	0.00515	0.01882	0.00025	222	66	126	5	120	2
19L11-1-15	80	80	1.00	0.07447	0.00908	0.18551	0.01757	0.01891	0.00061	1054	139	173	15	121	4

19L11-1-16	1330	1141	1.17	0.04752	0.00231	0.12582	0.00696	0.01901	0.00032	75	91	120	6	121	2
19L11-1-17	40	48	0.83	0.08752	0.01288	0.22096	0.02411	0.01886	0.00110	1372	123	203	20	120	7
19L11-1-18	45	56	0.81	0.06252	0.00923	0.16402	0.02533	0.01899	0.00121	692	225	154	22	121	8
19L11-1-19	95	103	0.92	0.07333	0.00553	0.17757	0.01263	0.01866	0.00052	1023	99	166	11	119	3
19L11-1-20	90	110	0.82	0.06282	0.00442	0.15984	0.01145	0.01891	0.00063	702	96	151	10	121	4
16L13-1-01	825	667	1.24	0.04897	0.00189	0.12673	0.00488	0.01873	0.00019	146	70	121	4	120	1
16L13-1-02	1288	1013	1.27	0.04652	0.00164	0.12027	0.00425	0.01869	0.00021	25	55	115	4	119	1
16L13-1-03	1463	483	3.03	0.05036	0.00261	0.12836	0.00629	0.01857	0.00023	212	91	123	6	119	1
16L13-1-04	1595	650	2.45	0.04763	0.00180	0.12158	0.00458	0.01852	0.00021	81	65	117	4	118	1
16L13-1-05	336	237	1.42	0.04742	0.00366	0.11812	0.00827	0.01850	0.00030	71	124	113	8	118	2
16L13-1-06	87	115	0.75	0.05016	0.00429	0.12434	0.00892	0.01877	0.00034	203	130	119	8	120	2
16L13-1-07	613	317	1.93	0.05097	0.00267	0.13270	0.00670	0.01906	0.00025	239	93	127	6	122	2
16L13-1-08	345	1038	0.33	0.05071	0.00159	0.13347	0.00426	0.01901	0.00016	227	58	127	4	121	1
16L13-1-09	503	310	1.62	0.04656	0.00239	0.12039	0.00614	0.01873	0.00024	27	85	115	6	120	2
16L13-1-10	1591	1122	1.42	0.04868	0.00140	0.12742	0.00373	0.01892	0.00017	133	52	122	3	121	1
16L13-1-11	316	333	0.95	0.04847	0.00248	0.12596	0.00633	0.01885	0.00021	122	93	120	6	120	1
16L13-1-12	121	146	0.83	0.05122	0.00270	0.22652	0.01195	0.03208	0.00042	251	98	207	10	204	3
16L13-1-13	1093	394	2.77	0.04798	0.00531	0.12250	0.01397	0.01836	0.00069	98	184	117	13	117	4
16L13-1-14	3294	1069	3.08	0.04834	0.00168	0.12328	0.00428	0.01850	0.00020	116	61	118	4	118	1
16L13-1-15	1678	691	2.43	0.04019	0.00303	0.10219	0.00695	0.01852	0.00037	-279	119	99	6	118	2
16L13-1-16	369	311	1.19	0.05082	0.00275	0.13088	0.00709	0.01864	0.00024	233	101	125	6	119	2
16L13-1-17	966	552	1.75	0.04536	0.00168	0.11484	0.00412	0.01842	0.00021	-2	53	110	4	118	1
16L13-1-18	754	206	3.66	0.05120	0.00383	0.12787	0.00922	0.01841	0.00041	250	123	122	8	118	3
17L02-1-01	80	15	5.42	0.05403	0.00761	0.13265	0.01350	0.01941	0.00064	372	170	126	12	124	4
17L02-1-02	92	16	5.85	0.05275	0.00495	0.13259	0.01082	0.01932	0.00055	318	134	126	10	123	3
17L02-1-03	75	15	5.03	0.04722	0.01064	0.12498	0.02783	0.01920	0.00066	60	382	120	25	123	4
17L02-1-04	133	19	6.95	0.05516	0.00520	0.13345	0.01015	0.01898	0.00054	419	119	127	9	121	3
17L02-1-05	225	28	8.14	0.05124	0.00772	0.12914	0.01491	0.01846	0.00059	252	201	123	13	118	4
17L02-1-06	89	17	5.27	0.05492	0.00579	0.12837	0.01044	0.01910	0.00059	409	127	123	9	122	4
17L02-1-07	58	12	4.93	0.04773	0.00852	0.13113	0.02189	0.01889	0.00096	86	250	125	20	121	6

17L02-1-08	295	33	8.82	0.05000	0.00746	0.13230	0.01707	0.01903	0.00070	195	222	126	15	122	4
17L02-1-09	58	12	4.78	0.05275	0.01287	0.13746	0.03549	0.01996	0.00130	318	387	131	32	127	8
17L02-1-10	108	18	6.10	0.05648	0.00728	0.13372	0.01218	0.01889	0.00065	471	141	127	11	121	4
17L02-1-11	208	30	6.95	0.05200	0.00493	0.14007	0.01307	0.01935	0.00066	285	149	133	12	124	4
17L02-1-12	151	22	6.98	0.05545	0.00733	0.12846	0.01164	0.01905	0.00060	431	146	123	10	122	4
17L02-1-13	244	30	8.14	0.05413	0.00699	0.13248	0.01350	0.01882	0.00079	376	154	126	12	120	5
17L02-1-14	111	18	6.24	0.05732	0.00553	0.14321	0.01115	0.01950	0.00054	504	123	136	10	125	3
17L02-1-15	192	27	7.01	0.05402	0.00620	0.13833	0.01332	0.01959	0.00063	372	159	132	12	125	4
17L02-1-16	81	18	4.57	0.05276	0.00627	0.12588	0.01382	0.01863	0.00067	319	181	120	12	119	4
17L02-1-17	165	38	4.29	0.05215	0.00729	0.13341	0.01590	0.01913	0.00075	292	196	127	14	122	5
17L02-1-18	173	28	6.25	0.05429	0.00709	0.14199	0.01489	0.02036	0.00054	383	188	135	13	130	3
17L02-1-19	350	45	7.72	0.05147	0.00484	0.13008	0.01155	0.01878	0.00049	262	153	124	10	120	3
17L02-1-20	61	12	5.26	0.05259	0.00727	0.13268	0.01358	0.01936	0.00075	311	161	127	12	124	5
17L02-1-21	124	23	5.38	0.05279	0.00570	0.12995	0.01260	0.01904	0.00059	320	163	124	11	122	4
17L02-1-O-01	87	25	3.46	0.18274	0.04112	0.41180	0.07167	0.01883	0.00087	2678	233	350	52	120	5
17L02-1-O-02	93	28	3.38	0.08853	0.03384	0.21307	0.08062	0.01746	0.00094	1394	846	196	67	112	6
17L02-1-O-03	289	71	4.07	0.06726	0.00704	0.16284	0.01389	0.01918	0.00051	846	133	153	12	122	3
17L02-1-O-04	127	26	4.96	0.13547	0.02933	0.34828	0.06684	0.01858	0.00119	2170	252	303	50	119	8
17L02-1-O-05	90	26	3.40	0.10380	0.03478	0.25689	0.08433	0.01795	0.00121	1693	746	232	68	115	8
17L02-1-O-06	187	43	4.31	0.11162	0.01714	0.27630	0.03927	0.01911	0.00085	1826	196	248	31	122	5
17L02-1-O-07	501	76	6.54	0.06817	0.00833	0.16655	0.01844	0.01931	0.00065	874	175	156	16	123	4
17L02-1-O-08	66	26	2.56	0.15880	0.02455	0.35494	0.04821	0.01913	0.00097	2443	162	308	36	122	6
17L02-1-O-09	160	37	4.36	0.06464	0.03421	0.15790	0.08283	0.01772	0.00123	763	1070	149	73	113	8
17L02-1-O-10	350	69	5.07	0.07992	0.01001	0.20308	0.02288	0.01910	0.00076	1195	161	188	19	122	5
17L02-1-O-11	54	17	3.13	0.22151	0.05359	0.41630	0.04593	0.01875	0.00121	2992	98	353	33	120	8
17L02-1-O-12	218	45	4.81	0.12366	0.02067	0.28217	0.03908	0.01891	0.00062	2010	203	252	31	121	4
17L02-1-O-13	359	108	3.31	0.05388	0.00460	0.13415	0.01052	0.01909	0.00045	366	134	128	9	122	3
17L02-1-O-14	304	65	4.66	0.09189	0.01480	0.24794	0.05089	0.01901	0.00063	1465	363	225	41	121	4
17L02-1-O-15	263	97	2.70	0.04605	0.00980	0.11825	0.02497	0.01863	0.00051	-	354	113	23	119	3
17L06-1-01	304	238	1.28	0.05452	0.00325	0.13725	0.00764	0.01869	0.00028	393	98	131	7	119	2

17L06-1-02	915	533	1.72	0.04875	0.00205	0.12944	0.00540	0.01927	0.00022	136	75	124	5	123	1
17L06-1-03	196	147	1.33	0.05180	0.00347	0.13633	0.00903	0.01933	0.00034	277	119	130	8	123	2
17L06-1-04	484	298	1.62	0.04545	0.00439	0.12270	0.01205	0.01927	0.00039	-31	177	118	11	123	2
17L06-1-05	801	496	1.62	0.05135	0.00241	0.13793	0.00631	0.01957	0.00023	257	84	131	6	125	1
17L06-1-06	307	346	0.89	0.05174	0.00294	0.13613	0.00783	0.01895	0.00021	274	112	130	7	121	1
17L06-1-07	70	81	0.86	0.05301	0.00495	0.12683	0.01590	0.01867	0.00040	329	244	121	14	119	3
17L06-1-08	365	247	1.48	0.05159	0.00442	0.13113	0.01055	0.01860	0.00040	267	143	125	9	119	3
17L06-1-09	625	505	1.24	0.04856	0.00336	0.13070	0.00866	0.01932	0.00032	126	118	125	8	123	2
17L06-1-10	253	196	1.29	0.04383	0.00509	0.11837	0.01294	0.01927	0.00045	-79	174	114	12	123	3
17L06-1-11	585	460	1.27	0.03894	0.00277	0.10324	0.00674	0.01904	0.00023	-352	156	100	6	122	1
17L06-1-12	582	321	1.81	0.04856	0.00332	0.12637	0.00804	0.01868	0.00022	127	120	121	7	119	1
17L06-1-13	180	137	1.32	0.04905	0.00402	0.12835	0.00997	0.01905	0.00040	150	135	123	9	122	3
17L06-1-14	1328	586	2.26	0.04930	0.00197	0.12794	0.00502	0.01867	0.00021	162	70	122	5	119	1
17L06-1-15	140	139	1.01	0.04848	0.00344	0.12801	0.00871	0.01936	0.00037	123	117	122	8	124	2
17L06-9-01	2199	873	2.52	0.04708	0.00173	0.12210	0.00424	0.01885	0.00023	53	55	117	4	120	1
17L06-9-02	577	398	1.45	0.05073	0.00194	0.13226	0.00500	0.01896	0.00027	229	61	126	4	121	2
17L06-9-03	202	199	1.01	0.05197	0.00317	0.12945	0.00661	0.01888	0.00037	284	81	124	6	121	2
17L06-9-04	2068	963	2.15	0.04633	0.00138	0.12170	0.00352	0.01895	0.00020	15	41	117	3	121	1
17L06-9-05	441	362	1.22	0.05134	0.00250	0.13292	0.00616	0.01892	0.00025	256	82	127	6	121	2
17L06-9-06	539	397	1.36	0.05695	0.00495	0.14768	0.01216	0.01892	0.00042	489	143	140	11	121	3
17L06-9-07	1287	831	1.55	0.05109	0.00186	0.13337	0.00485	0.01887	0.00030	245	54	127	4	121	2
17L06-9-08	165	137	1.21	0.06431	0.00816	0.16680	0.02272	0.01895	0.00084	752	216	157	20	121	5
17L06-9-09	83	154	0.54	0.05183	0.00577	0.12446	0.01179	0.01871	0.00058	278	157	119	11	119	4
17L06-9-10	599	463	1.29	0.05117	0.00789	0.13298	0.01792	0.01901	0.00041	248	261	127	16	121	3
17L06-9-11	199	258	0.77	0.05010	0.00293	0.13001	0.00735	0.01882	0.00029	200	101	124	7	120	2
17L06-9-12	870	570	1.53	0.05037	0.00187	0.13057	0.00479	0.01879	0.00024	212	62	125	4	120	1
17L06-9-13	1098	536	2.05	0.04769	0.00199	0.12345	0.00525	0.01888	0.00029	84	68	118	5	121	2
17L06-9-14	4990	1797	2.78	0.04718	0.00141	0.12297	0.00363	0.01883	0.00024	58	45	118	3	120	2
17L06-9-15	284	246	1.16	0.05080	0.00311	0.12826	0.00736	0.01878	0.00033	232	99	123	7	120	2
17L06-9-16	955	699	1.37	0.04994	0.00251	0.12829	0.00668	0.01852	0.00026	192	95	123	6	118	2

17L06-9-17	1250	653	1.92	0.04922	0.00180	0.12670	0.00435	0.01873	0.00022	158	58	121	4	120	1
17L06-9-18	271	255	1.07	0.04954	0.00453	0.12461	0.01075	0.01848	0.00046	174	148	119	10	118	3
17L06-9-19	1232	669	1.84	0.04764	0.00249	0.12407	0.00657	0.01884	0.00029	82	88	119	6	120	2
17L06-9-20	375	276	1.36	0.04984	0.00648	0.12411	0.01225	0.01888	0.00091	188	136	119	11	121	6
DD17-1-O-01	422	423	1.00	0.04489	0.00157	0.12348	0.00482	0.01974	0.00028	-25	54	118	4	126	2
DD17-1-O-02	555	460	1.21	0.04767	0.00107	0.12738	0.00290	0.01927	0.00019	83	35	122	3	123	1
DD17-1-O-03	272	279	0.98	0.04938	0.00129	0.13143	0.00332	0.01926	0.00020	166	39	125	3	123	1
DD17-1-O-04	704	462	1.52	0.04796	0.00110	0.12841	0.00266	0.01943	0.00021	97	29	123	2	124	1
DD17-1-O-05	560	405	1.38	0.05568	0.00175	0.15274	0.00658	0.01947	0.00033	440	65	144	6	124	2
DD17-1-O-06	185	377	0.49	0.04913	0.00112	0.13227	0.00321	0.01944	0.00021	154	37	126	3	124	1
DD17-1-O-07	252	306	0.82	0.04571	0.00123	0.12441	0.00327	0.01978	0.00028	-17	28	119	3	126	2
DD17-1-O-08	360	370	0.97	0.04790	0.00111	0.12877	0.00309	0.01945	0.00019	95	38	123	3	124	1
DD17-1-O-09	697	468	1.49	0.04463	0.00111	0.12109	0.00320	0.01971	0.00027	-38	30	116	3	126	2
DD17-1-O-10	98	162	0.60	0.05135	0.00244	0.13553	0.00641	0.01924	0.00033	256	77	129	6	123	2
DD17-1-O-11	382	314	1.22	0.04660	0.00138	0.12732	0.00400	0.01985	0.00031	29	40	122	4	127	2
DD17-1-O-12	330	292	1.13	0.05087	0.00145	0.13509	0.00380	0.01929	0.00019	235	47	129	3	123	1
DD17-1-O-13	404	364	1.11	0.04809	0.00117	0.12854	0.00324	0.01937	0.00022	104	38	123	3	124	1
DD17-1-O-14	278	254	1.09	0.04881	0.00147	0.13271	0.00430	0.01963	0.00023	139	54	127	4	125	1
DD17-1-O-15	420	372	1.13	0.04726	0.00128	0.12546	0.00347	0.01926	0.00024	63	42	120	3	123	2
DD17-1-O-16	324	304	1.06	0.05443	0.00383	0.14170	0.00808	0.01983	0.00082	389	61	135	7	127	5
DD17-1-O-17	140	239	0.59	0.04809	0.00170	0.12801	0.00528	0.01940	0.00065	104	44	122	5	124	4
DD17-1-O-18	268	258	1.04	0.04947	0.00169	0.13190	0.00484	0.01929	0.00032	170	55	126	4	123	2
DD17-1-O-19	2161	1042	2.07	0.04857	0.00077	0.13255	0.00235	0.01970	0.00018	127	25	126	2	126	1
DD17-1-O-20	189	278	0.68	0.05340	0.00235	0.14215	0.00559	0.01944	0.00024	346	67	135	5	124	2

Table S2. Major and trace element data for the Early Cretaceous appinites.

Sample	16L03-1	16L03-2	16L03-3	16L03-12	16L05-1	16L05-3	16L05-4	19L11-1	19L11-2	19L11-3	16L13-1	16L13-4	16L13-5	16L13-6	17L02-1	17L02-2	17L02-3	17L06-1	17L06-5	17L06-6	17L06-7	17L06-9
Lithology	appinites				appinites			appinites			appinites				appinites			appinites				
Pluton	Yangmuchuan				Qinggouzi			Caojiapuzi			Yingwugou				Dongshanzui			Qianrentun				
SiO_2	45.16	46.86	46.24	45.15	50.28	51.13	51.94	46.16	45.65	45.97	46.82	48.24	48.36	48.03	49.83	49.41	49.82	52.91	47.19	47.30	46.99	48.22
TiO_2	1.80	1.54	1.55	1.81	0.54	0.41	0.46	1.40	1.43	1.23	0.28	0.26	0.26	0.22	1.92	1.89	1.96	0.51	1.76	1.89	2.05	1.63
Al_2O_3	13.06	12.84	13.83	13.03	12.64	13.15	12.73	18.16	18.07	18.40	15.30	16.99	17.01	18.21	15.72	15.99	15.66	8.78	10.72	11.18	11.61	10.02
TFe_2O_3	18.24	15.49	14.62	18.74	8.63	8.00	8.42	11.04	11.43	11.16	7.00	7.15	7.19	6.82	9.61	9.71	9.60	8.72	9.27	9.61	9.52	9.48
MnO	0.23	0.23	0.23	0.23	0.13	0.13	0.13	0.11	0.12	0.11	0.12	0.10	0.10	0.10	0.08	0.08	0.08	0.15	0.11	0.12	0.11	0.13
MgO	5.98	7.10	8.39	6.00	11.90	11.23	11.58	7.44	7.67	7.45	10.45	10.94	11.02	9.70	7.99	7.92	8.00	12.91	14.40	14.14	13.46	14.63
CaO	8.21	10.34	8.84	8.47	10.92	9.83	10.14	9.85	9.77	9.47	16.50	11.57	11.61	12.21	8.88	8.85	8.83	10.32	11.83	11.49	11.40	11.55
Na_2O	3.55	2.72	2.63	3.22	1.95	2.09	1.92	2.20	2.24	2.12	0.51	1.41	1.41	1.27	2.84	2.90	2.84	1.69	1.84	2.09	1.94	1.50
K_2O	1.33	1.46	1.48	1.43	0.86	1.26	1.06	0.71	1.07	1.13	0.14	0.98	0.97	0.90	1.87	1.88	1.87	1.81	0.93	0.81	1.21	0.87
P_2O_5	0.15	0.13	0.11	0.16	0.09	0.08	0.09	0.05	0.06	0.09	0.04	0.04	0.04	0.04	0.09	0.12	0.07	0.35	0.10	0.11	0.11	0.11
LOI	1.85	1.09	1.81	1.44	1.76	1.94	1.73	2.53	2.44	2.78	2.66	2.42	2.45	2.30	0.95	0.97	0.97	1.52	1.15	1.10	1.06	1.41
Total	99.57	99.80	99.72	99.68	99.69	99.25	100.18	99.65	99.94	99.91	99.79	100.10	100.44	99.81	99.78	99.72	99.70	99.68	99.29	99.82	99.47	99.55
$Mg^{\#}$	40	48	53	39	73	74	73	57	57	57	75	75	75	74	62	62	62	75	76	75	74	76
Sc	44.03	49.59	52.69	43.30	31.71	29.71	30.31	32.57	33.37	28.96	27.42	32.93	30.90	23.12	44.13	42.47	44.83	35.41	53.65	52.63	52.56	53.52
V	392	400	330	404	135	115	123	321	332	303	121	118	115	101	361	362	366	137	337	364	384	334
Cr	15.11	77.76	292.35	15.27	354.24	315.50	330.74	35.94	36.50	37.70	231.19	229.59	226.00	213.15	103.61	116.35	105.59	785.66	544.08	275.71	259.21	297.78
Co	58.28	49.21	42.44	59.43	43.48	38.86	41.05	46.74	46.17	44.90	34.14	42.18	41.50	41.03	38.43	37.38	39.23	39.88	58.01	56.27	60.01	59.99
Ni	43.24	46.59	65.15	44.27	78.53	71.39	76.60	26.72	26.58	26.22	36.60	41.30	40.90	44.28	29.60	32.14	29.60	164.79	168.14	96.42	111.75	135.61
Cu	25.06	6.31	7.84	26.15	20.60	16.74	21.81	26.79	24.39	20.96	5.24	21.74	22.30	25.14	32.54	41.20	30.64	10.72	57.75	59.17	55.98	57.94
Zn	111.49	109.79	142.52	107.94	63.65	62.48	62.39	82.41	86.15	91.54	53.58	49.87	48.70	47.68	83.07	80.55	79.77	97.80	53.54	57.15	56.57	59.00
Ga	21.55	18.29	23.74	21.45	14.88	14.68	14.67	21.42	21.03	21.87	19.98	15.87	16.10	16.25	22.78	22.82	22.40	16.02	13.65	14.44	14.65	12.96
Rb	35.78	37.72	37.12	41.64	19.70	38.91	28.20	18.46	28.41	34.10	3.79	49.59	48.90	44.43	49.30	54.07	49.85	27.72	11.15	9.02	17.68	10.22
Sr	547	448	455	536	545	591	539	697	672	687	525	705	720	743	557	585	552	367	520	490	461	408
Y	29.93	25.63	40.60	27.42	15.88	14.10	14.37	16.10	16.16	14.47	7.39	6.80	6.03	5.95	28.50	24.28	28.02	16.72	22.79	23.13	25.02	20.88
Zr	66.28	51.94	108.47	72.70	58.29	71.17	76.63	51.85	50.53	49.28	39.35	39.62	38.66	38.55	46.41	77.15	55.93	161.17	76.36	75.14	72.26	73.13

Nb	8.33	5.18	12.84	7.75	4.11	3.43	3.67	4.24	4.08	3.68	2.19	1.44	1.32	1.23	8.42	7.28	8.27	4.15	5.72	6.43	6.89	5.86
Cs	0.25	0.40	0.31	0.30	0.33	0.44	0.38	0.62	1.69	2.27	0.12	1.21	1.32	1.45	0.35	0.47	0.38	0.08	0.03	0.04	0.04	0.06
Ba	215	216	383	258	333	384	377	249	315	324	13	204	201	197	646	672	636	414	400	346	524	434
La	22.67	13.20	38.03	22.18	15.89	17.23	16.15	12.13	12.03	12.43	8.14	8.83	8.79	8.74	39.71	35.53	40.43	42.09	14.73	16.42	16.30	14.83
Ce	48.95	23.74	100.65	45.60	32.62	30.30	31.05	28.56	26.70	26.00	16.28	16.88	16.45	16.55	88.39	74.90	88.43	92.47	40.14	43.58	44.06	39.28
Pr	5.61	2.91	13.13	5.02	3.99	3.64	3.67	3.71	3.59	3.49	2.03	2.05	2.01	1.97	11.08	9.22	10.83	11.97	6.02	6.35	6.33	5.69
Nd	20.45	12.73	50.74	18.15	16.47	14.28	14.59	16.55	16.35	14.95	8.03	8.17	8.07	7.61	45.60	37.07	43.77	50.89	29.49	30.63	31.28	28.02
Sm	4.61	3.48	9.50	4.16	3.57	3.09	3.12	3.84	3.71	3.57	1.76	1.69	1.59	1.50	9.16	7.48	8.57	9.01	6.93	6.99	7.40	6.68
Eu	1.64	1.33	3.10	1.54	1.04	0.88	0.92	1.24	1.23	1.18	0.65	0.69	0.65	0.63	2.31	2.00	2.24	2.24	1.92	1.87	2.04	1.75
Gd	4.79	4.26	7.67	4.54	3.18	2.73	2.84	3.71	3.77	3.13	1.63	1.53	1.49	1.45	7.84	6.57	7.25	6.33	6.29	6.50	6.98	5.86
Tb	0.88	0.79	1.22	0.86	0.48	0.41	0.44	0.57	0.56	0.49	0.25	0.23	0.22	0.21	1.16	0.96	1.05	0.73	0.89	0.90	0.90	0.80
Dy	5.21	4.72	7.17	5.12	2.95	2.54	2.60	3.19	3.29	2.97	1.39	1.33	1.25	1.16	5.73	4.85	5.53	3.72	4.68	4.61	5.00	4.40
Ho	1.08	0.97	1.41	1.02	0.58	0.48	0.51	0.57	0.64	0.55	0.28	0.26	0.24	0.23	1.08	0.93	1.06	0.63	0.92	0.94	0.92	0.82
Er	2.86	2.63	4.02	2.85	1.63	1.38	1.43	1.60	1.64	1.45	0.78	0.67	0.65	0.62	2.82	2.40	2.79	1.69	2.30	2.31	2.39	2.12
Tm	0.42	0.40	0.60	0.42	0.23	0.20	0.21	0.22	0.22	0.20	0.11	0.09	0.09	0.08	0.38	0.33	0.36	0.22	0.30	0.31	0.29	0.27
Yb	2.72	2.48	3.68	2.63	1.38	1.26	1.29	1.36	1.39	1.28	0.70	0.58	0.56	0.55	2.03	1.90	2.08	1.32	1.78	1.92	1.88	1.71
Lu	0.38	0.38	0.57	0.39	0.21	0.18	0.19	0.19	0.19	0.17	0.10	0.09	0.08	0.08	0.28	0.25	0.27	0.18	0.25	0.25	0.25	0.24
Hf	2.35	1.76	3.51	2.45	1.80	1.91	2.02	1.65	1.62	1.62	1.06	1.12	1.03	1.01	2.18	2.71	2.31	4.10	2.29	2.33	2.34	2.17
Ta	0.48	0.35	0.52	0.52	0.22	0.20	0.21	0.18	0.21	0.18	0.10	0.07	0.06	0.07	0.29	0.23	0.30	0.16	0.25	0.28	0.32	0.25
Pb	5.27	4.34	4.90	5.67	5.60	5.22	4.68	3.98	3.52	3.38	4.88	4.45	4.49	4.51	6.69	6.55	6.80	3.13	1.82	2.39	2.02	1.72
Th	2.31	1.71	2.01	3.08	2.12	3.35	3.11	1.79	1.78	1.72	1.44	1.98	1.80	1.79	5.86	5.04	6.31	3.86	1.41	1.53	1.26	1.42
U	0.59	0.51	0.51	0.82	0.38	0.62	0.47	0.31	0.30	0.38	0.26	0.28	0.25	0.23	0.33	0.33	0.34	0.56	0.24	0.24	0.17	0.30
∑REE	122.27	74.01	241.48	114.47	84.21	78.61	79.01	77.44	75.32	71.85	42.11	43.09	42.14	41.36	217.57	184.40	214.67	223.49	116.62	123.60	126.01	112.47
∑LREE	103.93	57.39	215.13	96.65	73.58	69.42	69.50	66.03	63.62	61.61	36.89	38.31	37.56	37.00	196.26	166.19	194.27	208.66	99.22	105.85	107.40	96.24
∑HREE	18.34	16.62	26.35	17.83	10.63	9.19	9.52	11.41	11.70	10.24	5.22	4.78	4.58	4.36	21.31	18.20	20.40	14.83	17.41	17.74	18.61	16.22
∑LREE/∑HREE	5.67	3.45	8.16	5.42	6.92	7.56	7.30	5.78	5.44	6.02	7.06	8.01	8.20	8.48	9.21	9.13	9.53	14.07	5.70	5.97	5.77	5.93
Yb_N	13.00	11.86	17.61	12.59	6.59	6.04	6.15	6.52	6.67	6.11	3.33	2.76	2.68	2.62	9.72	9.08	9.96	6.33	8.51	9.18	9.00	8.18
$(La/Yb)_N$	5.63	3.59	6.97	5.68	7.78	9.20	8.47	6.00	5.81	6.56	7.87	10.33	10.58	10.77	13.18	12.62	13.10	21.45	5.58	5.77	5.84	5.85
Eu/Eu*	1.06	1.06	1.08	1.08	0.92	0.91	0.93	0.99	1.00	1.05	1.15	1.28	1.27	1.29	0.81	0.85	0.85	0.86	0.87	0.84	0.86	0.84
Th/U	3.90	3.36	3.96	3.76	5.61	5.40	6.65	5.83	5.87	4.57	5.60	7.13	7.20	7.71	17.95	15.38	18.83	6.86	5.91	6.46	7.24	4.69

Note: LOI: Loss on ignition; $Mg^{\#}=Mg^{2+}/(Mg^{2+}+TFe^{2+})$; $\delta Eu=(Eu)_N/[(Gd)_N*(Sm)_N]/2$; $(La/Yb)_N=(La/0.310)/(Yb/0.209)$; $Yb_N=Yb/0.209$

Table S3. Whole-rock Sr-Nd-Pb isotopic data for Early Cretaceous appinites.

Pluton and sample	$^{87}Rb/^{86}Sr$	$^{87}Sr/^{86}Sr$	2σ	$(^{87}Sr/^{86}Sr)_i$	$^{147}Sm/^{144}Nd$	$^{143}Nd/^{144}Nd$	2σ	Age (Ma)	$\varepsilon_{Nd}(0)$	$\varepsilon_{Nd}(t)$	$f_{Sm/Nd}$	T_{DM1} (Ma)	T_{DM2} (Ma)	$^{206}Pb/^{204}Pb$	$^{207}Pb/^{204}Pb$	$^{208}Pb/^{204}Pb$	$(^{206}Pb/^{204}Pb)_i$	$(^{207}Pb/^{204}Pb)_i$	$(^{208}Pb/^{204}Pb)_i$
Qinggouzi appinites																			
16L05-1	0.104276	0.711159	0.000010	0.7110	0.1312	0.511889	0.000010	125	-14.61	-13.57	-0.33	2318	2013	18.265	15.649	39.138	18.180	15.644	38.983
16L05-4	0.150881	0.711279	0.000009	0.7110	0.1296	0.511888	0.000010	125	-14.62	-13.56	-0.34	2277	2013	18.476	15.678	39.429	18.350	15.672	39.155
16L05-3	0.020874	0.711351	0.000007	0.7113	0.1310	0.511888	0.000010	125	-14.62	-13.58	-0.33	2315	2014	18.441	15.665	39.366	18.375	15.662	39.244
Dongshanzui appinites																			
17L02-1	0.255258	0.716738	0.000008	0.7163	0.1216	0.511333	0.000005	121	-25.46	-24.30	-0.38	2986	2879	16.141	15.267	40.092	16.083	15.264	39.751
17L02-2	0.266914	0.716761	0.000010	0.7163	0.1221	0.511339	0.000005	121	-25.34	-24.19	-0.38	2994	2870	16.233	15.289	39.761	16.174	15.287	39.463
17L02-3	0.260883	0.716730	0.000008	0.7163	0.1184	0.511345	0.000005	121	-25.22	-24.02	-0.40	2869	2858	16.146	15.252	40.099	16.087	15.249	39.738
Qianrentun appinites																			
17L06-5	0.061921	0.707166	0.000006	0.7071	0.1421	0.512250	0.000005	120	-7.57	-6.74	-0.28	1911	1454	17.439	15.531	38.061	17.287	15.523	37.766
17L06-6	0.053156	0.707347	0.000005	0.7073	0.1381	0.512239	0.000005	120	-7.78	-6.89	-0.30	1831	1468	17.380	15.537	38.021	17.264	15.531	37.777
17L06-7	0.110629	0.707573	0.000007	0.7074	0.1430	0.512242	0.000004	120	-7.72	-6.90	-0.27	1952	1467	17.128	15.502	37.796	17.028	15.498	37.559

Table S4. In situ zircon Hf-O isotopic data for Early Cretaceous appinites.

Spot no.	Age (Ma)	$^{176}Yb/^{177}Hf$	2σ	$^{176}Lu/^{177}Hf$	2σ	$^{176}Hf/^{177}Hf$	2σ	$\varepsilon_{Hf}(0)$	$\varepsilon_{Hf}(t)$	2σ	T_{DM1} (Ma)	T_{DM2} (Ma)	$f_{Lu/Hf}$	$\delta^{18}O$	2σ
16L03-1-01	120	0.031500	0.000200	0.001210	0.000006	0.282167	0.000012	-21.40	-18.85	0.4	1538	2373	-0.96	-	-
16L03-1-02	120	0.026582	0.000459	0.001065	0.000017	0.282167	0.000012	-21.41	-18.88	0.4	1532	2373	-0.97	-	-
16L03-1-03	120	0.030425	0.001968	0.001237	0.000075	0.282134	0.000012	-22.58	-20.05	0.4	1585	2447	-0.96	-	-
16L03-1-04	120	0.019618	0.000423	0.000817	0.000015	0.282155	0.000013	-21.83	-19.27	0.5	1539	2399	-0.98	-	-
16L03-1-05	120	0.028082	0.000267	0.001138	0.000010	0.282162	0.000011	-21.57	-19.06	0.4	1542	2384	-0.97	-	-
16L03-1-06	120	0.020476	0.000515	0.000896	0.000014	0.282206	0.000012	-20.01	-17.30	0.4	1470	2280	-0.97	-	-
16L03-1-07	120	0.020330	0.000550	0.000878	0.000019	0.282185	0.000012	-20.77	-18.12	0.4	1499	2330	-0.97	-	-
16L03-1-08	120	0.022378	0.000287	0.000904	0.000016	0.282208	0.000014	-19.94	-17.29	0.5	1468	2277	-0.97	-	-
16L03-1-09	120	0.017758	0.000636	0.000732	0.000022	0.282260	0.000014	-18.12	-15.59	0.5	1390	2166	-0.98	-	-
16L03-1-10	120	0.025801	0.000801	0.000995	0.000024	0.282148	0.000012	-22.06	-19.53	0.4	1555	2414	-0.97	-	-
16L03-1-11	120	0.030319	0.001714	0.001253	0.000059	0.282362	0.000015	-14.51	-11.96	0.5	1266	1939	-0.96	-	-
16L03-1-12	120	0.015775	0.000914	0.000663	0.000032	0.282181	0.000012	-20.89	-18.38	0.4	1496	2340	-0.98	-	-
16L03-1-13	120	0.025448	0.000949	0.000989	0.000032	0.282138	0.000011	-22.41	-19.84	0.4	1569	2435	-0.97	-	-
16L03-1-14	120	0.013810	0.000158	0.000560	0.000007	0.282129	0.000012	-22.72	-20.14	0.4	1563	2454	-0.98	-	-
16L03-1-15	120	0.021444	0.000539	0.000883	0.000018	0.282171	0.000013	-21.26	-18.68	0.5	1519	2362	-0.97	-	-
16L05-1-01	125	0.072273	0.000925	0.002275	0.000027	0.282207	0.000019	-19.98	-17.41	0.7	1525	2285	-0.93	8.15	0.27
16L05-1-02	125	0.020962	0.000423	0.000664	0.000014	0.282241	0.000013	-18.78	-16.11	0.5	1413	2203	-0.98	8.31	0.22
16L05-1-03	125	0.033728	0.001308	0.001037	0.000037	0.282211	0.000011	-19.83	-17.18	0.4	1469	2270	-0.97	8.11	0.28
16L05-1-04	125	0.075087	0.005518	0.002242	0.000149	0.282253	0.000012	-18.37	-15.80	0.4	1458	2183	-0.93	8.24	0.31
16L05-1-05	125	0.059188	0.000323	0.001902	0.000007	0.282261	0.000015	-18.06	-15.48	0.5	1432	2163	-0.94	8.56	0.22
16L05-1-06	125	0.050693	0.002145	0.001593	0.000058	0.282233	0.000012	-19.06	-16.48	0.4	1460	2225	-0.95	8.02	0.14
16L05-1-07	125	0.064530	0.000469	0.001894	0.000010	0.282212	0.000013	-19.80	-17.20	0.5	1501	2272	-0.94	8.54	0.18
16L05-1-08	125	0.014902	0.000703	0.000465	0.000019	0.282253	0.000012	-18.35	-15.65	0.4	1389	2175	-0.99	8.03	0.21
16L05-1-09	125	0.068029	0.001603	0.002077	0.000042	0.282242	0.000012	-18.73	-16.14	0.4	1466	2205	-0.94	7.90	0.23
16L05-1-10	125	0.039270	0.000647	0.001300	0.000018	0.282247	0.000015	-18.58	-15.93	0.5	1429	2193	-0.96	8.24	0.23
16L05-1-11	125	0.054278	0.000358	0.002184	0.000008	0.282238	0.000013	-18.89	-16.29	0.5	1476	2216	-0.93	8.08	0.23
16L05-1-12	125	0.051235	0.002271	0.002029	0.000087	0.282214	0.000014	-19.72	-17.17	0.5	1504	2269	-0.94	6.33	0.29

16L05-1-13	125	0.042284	0.000558	0.001672	0.000021	0.282223	0.000013	-19.40	-16.82	0.5	1477	2247	-0.95	8.16	0.19
16L05-1-14	125	0.010366	0.000065	0.000466	0.000003	0.282261	0.000013	-18.07	-15.37	0.5	1379	2157	-0.99	8.06	0.14
16L05-1-15	125	0.011448	0.000103	0.000554	0.000007	0.282247	0.000022	-18.58	-15.88	0.8	1401	2189	-0.98	7.85	0.28
19L11-1-01	120	0.029798	0.000081	0.000982	0.000006	0.282135	0.000009	-22.51	-19.96	0.3	1572	2442	-0.97	7.40	0.17
19L11-1-02	120	0.061248	0.000787	0.001913	0.000021	0.282121	0.000009	-23.02	-20.54	0.3	1632	2478	-0.94	7.30	0.12
19L11-1-03	120	0.054004	0.000290	0.001687	0.000012	0.282094	0.000009	-23.97	-21.48	0.3	1660	2537	-0.95	7.79	0.14
19L11-1-04	120	0.019883	0.000180	0.000674	0.000004	0.282116	0.000009	-23.21	-20.64	0.3	1587	2485	-0.98	7.55	0.20
19L11-1-05	120	0.014974	0.000168	0.000469	0.000003	0.282135	0.000010	-22.52	-19.93	0.3	1551	2440	-0.99	7.40	0.21
19L11-1-06	120	0.056474	0.000266	0.001785	0.000010	0.282095	0.000009	-23.95	-21.47	0.3	1664	2536	-0.95	7.35	0.25
19L11-1-07	120	0.024661	0.000175	0.000839	0.000005	0.282117	0.000009	-23.18	-20.62	0.3	1592	2483	-0.97	7.69	0.21
19L11-1-08	120	0.045437	0.000358	0.001450	0.000015	0.282084	0.000008	-24.35	-21.84	0.3	1665	2559	-0.96	7.53	0.22
19L11-1-09	120	0.015028	0.000152	0.000508	0.000008	0.282111	0.000009	-23.38	-20.79	0.3	1586	2494	-0.98	7.71	0.20
19L11-1-10	120	0.045399	0.000491	0.001439	0.000018	0.282093	0.000008	-24.03	-21.52	0.3	1652	2539	-0.96	7.46	0.16
19L11-1-11	120	0.021840	0.000197	0.000766	0.000004	0.282137	0.000009	-22.46	-19.89	0.3	1561	2438	-0.98	7.20	0.18
19L11-1-12	120	0.026900	0.000460	0.000868	0.000015	0.282100	0.000008	-23.77	-21.21	0.3	1617	2521	-0.97	7.35	0.24
19L11-1-13	120	0.016380	0.000274	0.000534	0.000007	0.282094	0.000009	-23.97	-21.39	0.3	1611	2532	-0.98	7.37	0.14
19L11-1-14	120	0.011455	0.000147	0.000393	0.000005	0.282094	0.000009	-23.99	-21.39	0.3	1605	2532	-0.99	7.49	0.25
19L11-1-15	120	0.033351	0.000769	0.001101	0.000026	0.282087	0.000008	-24.21	-21.67	0.3	1644	2549	-0.97	7.53	0.18
16L13-1-01	119	0.004569	0.000030	0.000195	0.000001	0.282264	0.000018	-17.97	-15.34	0.6	1365	2152	-0.99	-	-
16L13-1-02	119	0.007322	0.000463	0.000316	0.000018	0.282242	0.000017	-18.75	-16.17	0.6	1400	2203	-0.99	-	-
16L13-1-03	119	0.024133	0.000541	0.000765	0.000018	0.282204	0.000014	-20.09	-17.52	0.5	1468	2289	-0.98	-	-
16L13-1-04	119	0.014810	0.000495	0.000507	0.000014	0.282232	0.000016	-19.10	-16.51	0.6	1420	2225	-0.98	-	-
16L13-1-05	119	0.003488	0.000073	0.000135	0.000002	0.282246	0.000016	-18.61	-16.02	0.6	1388	2194	-1.00	-	-
16L13-1-06	119	0.011932	0.000129	0.000497	0.000005	0.282356	0.000014	-14.71	-11.97	0.5	1249	1944	-0.99	-	-
16L13-1-07	119	0.008395	0.000126	0.000290	0.000004	0.282224	0.000015	-19.38	-16.69	0.5	1423	2239	-0.99	-	-
16L13-1-08	119	0.023619	0.001730	0.001254	0.000097	0.282213	0.000017	-19.77	-17.16	0.6	1475	2268	-0.96	-	-
16L13-1-09	119	0.004958	0.000368	0.000178	0.000013	0.282291	0.000020	-17.03	-14.45	0.7	1328	2094	-0.99	-	-
16L13-1-10	119	0.007842	0.000198	0.000327	0.000010	0.282259	0.000014	-18.15	-15.57	0.5	1377	2165	-0.99	-	-
16L13-1-11	119	0.006322	0.000191	0.000278	0.000008	0.282257	0.000014	-18.23	-15.60	0.5	1378	2169	-0.99	-	-
16L13-1-12	119	0.008048	0.000150	0.000276	0.000006	0.282255	0.000011	-18.27	-15.73	0.4	1379	2174	-0.99	-	-
16L13-1-13	119	0.005218	0.000037	0.000181	0.000001	0.282261	0.000015	-18.08	-15.45	0.5	1369	2159	-0.99	-	-
16L13-1-14	119	0.005391	0.000232	0.000186	0.000008	0.282247	0.000012	-18.56	-15.95	0.4	1388	2190	-0.99	-	-
16L13-1-15	119	0.008187	0.000338	0.000327	0.000013	0.282242	0.000014	-18.74	-16.11	0.5	1400	2201	-0.99	-	-
17L02-1-O-01	123	0.010113	0.000275	0.000310	0.000007	0.281750	0.000018	-36.14	-33.47	0.6	2069	3290	-0.99	5.76	0.36
17L02-1-O-02	123	0.031890	0.000642	0.000954	0.000023	0.281748	0.000018	-36.23	-33.62	0.6	2107	3298	-0.97	5.68	0.31

17L02-1-O-03	123	0.012044	0.000114	0.000381	0.000006	0.281754	0.000017	-36.00	-33.34	0.6	2067	3282	-0.99	5.55	0.28
17L02-1-O-04	123	0.017879	0.000861	0.000525	0.000026	0.281760	0.000019	-35.79	-33.14	0.7	2067	3269	-0.98	5.64	0.21
17L02-1-O-05	123	0.012486	0.000148	0.000397	0.000004	0.281755	0.000018	-35.96	-33.30	0.6	2067	3279	-0.99	5.26	0.28
17L02-1-O-06	123	0.003715	0.000312	0.000133	0.000007	0.281760	0.000018	-35.79	-33.11	0.6	2046	3268	-1.00	6.05	0.25
17L02-1-O-07	123	0.014575	0.000202	0.000430	0.000004	0.281751	0.000017	-36.12	-33.46	0.6	2074	3289	-0.99	5.84	0.32
17L02-1-O-08	123	0.012946	0.000599	0.000401	0.000022	0.281758	0.000021	-35.86	-33.20	0.7	2063	3273	-0.99	5.95	0.22
17L02-1-O-09	123	0.014648	0.000204	0.000463	0.000008	0.281761	0.000020	-35.74	-33.09	0.7	2062	3266	-0.99	5.85	0.28
17L02-1-O-10	123	0.008582	0.000149	0.000266	0.000005	0.281753	0.000019	-36.03	-33.36	0.7	2062	3283	-0.99	6.02	0.20
17L02-1-O-11	123	0.027834	0.001992	0.000783	0.000061	0.281748	0.000021	-36.20	-33.57	0.7	2096	3295	-0.98	5.61	0.29
17L02-1-O-12	123	0.009566	0.000234	0.000292	0.000009	0.281760	0.000017	-35.80	-33.13	0.6	2055	3269	-0.99	6.17	0.20
17L02-1-O-13	123	0.016984	0.000477	0.000490	0.000013	0.281778	0.000019	-35.16	-32.51	0.7	2041	3230	-0.99	5.85	0.17
17L02-1-O-14	123	0.027463	0.002427	0.000788	0.000070	0.281740	0.000018	-36.48	-33.86	0.6	2108	3313	-0.98	5.52	0.34
17L02-1-O-15	123	0.019691	0.000505	0.000584	0.000013	0.281770	0.000017	-35.44	-32.80	0.6	2056	3248	-0.98	5.77	0.25
17L02-1-O-16	123	0.011034	0.000258	0.000326	0.000008	0.281742	0.000017	-36.43	-33.77	0.6	2081	3309	-0.99	5.91	0.23
17L02-1-01	121	0.010946	0.000696	0.000471	0.000032	0.281749	0.000017	-36.17	-33.58	0.6	2078	3294	-0.99	-	-
17L02-1-02	121	0.016448	0.001010	0.000690	0.000043	0.281749	0.000018	-36.19	-33.79	0.6	2091	3301	-0.98	-	-
17L02-1-03	121	0.013856	0.000129	0.000583	0.000005	0.281764	0.000016	-35.64	-33.01	0.6	2064	3260	-0.98	-	-
17L02-1-04	121	0.007650	0.000382	0.000309	0.000014	0.281772	0.000015	-35.37	-32.79	0.5	2039	3245	-0.99	-	-
17L02-1-05	121	0.011283	0.000240	0.000488	0.000012	0.281755	0.000018	-35.96	-33.49	0.7	2072	3285	-0.99	-	-
17L02-1-06	121	0.009473	0.000395	0.000397	0.000014	0.281770	0.000016	-35.42	-32.79	0.6	2046	3246	-0.99	-	-
17L02-1-07	121	0.028250	0.000524	0.001077	0.000018	0.281745	0.000018	-36.32	-33.72	0.6	2118	3304	-0.97	-	-
17L02-1-08	121	0.014875	0.000223	0.000598	0.000006	0.281756	0.000017	-35.92	-33.30	0.6	2076	3278	-0.98	-	-
17L02-1-09	121	0.020979	0.000949	0.000847	0.000039	0.281723	0.000017	-37.11	-34.70	0.6	2135	3359	-0.97	-	-
17L02-1-10	121	0.021657	0.000740	0.000885	0.000030	0.281764	0.000017	-35.64	-33.04	0.6	2080	3262	-0.97	-	-
17L02-1-11	121	0.008907	0.000694	0.000358	0.000027	0.281767	0.000018	-35.53	-32.94	0.6	2048	3255	-0.99	-	-
17L02-1-12	121	0.012340	0.000460	0.000520	0.000022	0.281761	0.000016	-35.75	-33.15	0.6	2065	3268	-0.98	-	-
17L02-1-13	121	0.015883	0.000135	0.000673	0.000007	0.281766	0.000016	-35.59	-32.98	0.6	2067	3258	-0.98	-	-
17L02-1-14	121	0.022698	0.000262	0.000906	0.000015	0.281756	0.000017	-35.93	-33.36	0.6	2093	3280	-0.97	-	-
17L02-1-15	121	0.019419	0.000484	0.000797	0.000025	0.281757	0.000016	-35.91	-33.37	0.6	2086	3280	-0.98	-	-
17L02-1-16	121	0.015712	0.000436	0.000577	0.000011	0.281760	0.000019	-35.78	-33.18	0.7	2069	3270	-0.98	-	-
17L02-1-17	121	0.014990	0.000915	0.000521	0.000033	0.281789	0.000020	-34.77	-32.17	0.7	2027	3207	-0.98	-	-
17L02-1-18	121	0.005486	0.000060	0.000199	0.000002	0.281751	0.000018	-36.12	-33.49	0.6	2062	3290	-0.99	-	-
17L02-1-19	121	0.007546	0.000169	0.000298	0.000006	0.281787	0.000017	-34.83	-32.21	0.6	2018	3210	-0.99	-	-
17L02-1-20	121	0.012900	0.000666	0.000490	0.000028	0.281772	0.000017	-35.37	-32.77	0.6	2049	3244	-0.99	-	-
17L06-1-01	122	0.024287	0.002201	0.000980	0.000077	0.282552	0.000018	-7.78	-5.24	0.6	990	1511	-0.97	-	-
17L06-1-02	122	0.048677	0.000438	0.001903	0.000007	0.282533	0.000019	-8.45	-5.90	0.7	1042	1556	-0.94	-	-
17L06-1-03	122	0.012432	0.000166	0.000518	0.000006	0.282563	0.000020	-7.40	-4.75	0.7	963	1483	-0.98	-	-

17L06-1-04	122	0.028882	0.000402	0.001178	0.000018	0.282542	0.000021	-8.14	-5.54	0.7	1010	1533	-0.96	-	-
17L06-1-05	122	0.032862	0.000017	0.001381	0.000002	0.282544	0.000024	-8.07	-5.44	0.8	1012	1528	-0.96	-	-
17L06-1-06	122	0.017905	0.000296	0.000757	0.000012	0.282605	0.000018	-5.90	-3.31	0.6	910	1390	-0.98	-	-
17L06-1-07	122	0.007961	0.000427	0.000348	0.000016	0.282564	0.000021	-7.35	-4.76	0.7	957	1481	-0.99	-	-
17L06-1-08	122	0.024041	0.000243	0.000996	0.000012	0.282542	0.000017	-8.13	-5.60	0.6	1004	1534	-0.97	-	-
17L06-1-09	122	0.004451	0.000441	0.000206	0.000019	0.282522	0.000018	-8.85	-6.17	0.6	1012	1573	-0.99	-	-
17L06-1-10	122	0.015970	0.000555	0.000666	0.000023	0.282570	0.000019	-7.14	-4.50	0.7	957	1467	-0.98	-	-
17L06-1-11	122	0.022320	0.000207	0.000959	0.000008	0.282555	0.000021	-7.68	-5.08	0.7	985	1503	-0.97	-	-
17L06-1-12	122	0.026403	0.001575	0.001077	0.000064	0.282519	0.000020	-8.96	-6.44	0.7	1039	1587	-0.97	-	-
17L06-1-13	122	0.014233	0.000536	0.000594	0.000020	0.282550	0.000024	-7.85	-5.22	0.8	983	1512	-0.98	-	-
17L06-1-14	122	0.053007	0.000241	0.002056	0.000012	0.282514	0.000020	-9.12	-6.68	0.7	1074	1602	-0.94	-	-
17L06-1-15	122	0.018473	0.000566	0.000793	0.000022	0.282571	0.000021	-7.10	-4.44	0.8	958	1464	-0.98	-	-
17L06-9-01	120	0.037467	0.000283	0.001164	0.000010	0.282427	0.000012	-12.19	-9.65	0.4	1171	1792	-0.96	6.29	0.20
17L06-9-02	120	0.038944	0.000068	0.001526	0.000004	0.282437	0.000009	-11.86	-9.35	0.3	1169	1773	-0.95	6.62	0.21
17L06-9-03	120	0.059407	0.001030	0.001744	0.000030	0.282435	0.000010	-11.92	-9.43	0.3	1178	1777	-0.95	6.43	0.19
17L06-9-04	120	0.022934	0.000787	0.000706	0.000024	0.282422	0.000008	-12.40	-9.82	0.3	1165	1803	-0.98	6.43	0.19
17L06-9-05	120	0.037070	0.000397	0.001123	0.000009	0.282436	0.000010	-11.90	-9.36	0.4	1158	1773	-0.97	6.16	0.22
17L06-9-06	120	0.025230	0.000513	0.000796	0.000015	0.282446	0.000011	-11.54	-8.97	0.4	1133	1749	-0.98	6.52	0.14
17L06-9-07	120	0.013719	0.000320	0.000478	0.000007	0.282455	0.000010	-11.20	-8.61	0.3	1111	1726	-0.99	6.66	0.25
17L06-9-08	120	0.040400	0.001100	0.001201	0.000032	0.282444	0.000011	-11.59	-9.06	0.4	1148	1754	-0.96	6.49	0.16
17L06-9-09	120	0.041100	0.000362	0.001296	0.000014	0.282439	0.000012	-11.78	-9.25	0.4	1158	1766	-0.96	6.47	0.18
17L06-9-10	120	0.023758	0.000176	0.000765	0.000004	0.282431	0.000011	-12.06	-9.49	0.4	1153	1782	-0.98	6.52	0.15
17L06-9-11	120	0.023920	0.000144	0.000776	0.000004	0.282433	0.000012	-11.98	-9.42	0.4	1151	1777	-0.98	6.52	0.17
17L06-9-12	120	0.035478	0.000501	0.001161	0.000017	0.282441	0.000012	-11.71	-9.17	0.4	1151	1761	-0.97	6.48	0.28
17L06-9-13	120	0.022235	0.000369	0.000683	0.000012	0.282446	0.000010	-11.53	-8.95	0.4	1130	1748	-0.98	6.52	0.15
17L06-9-14	120	0.021196	0.000360	0.000687	0.000012	0.282430	0.000010	-12.09	-9.52	0.3	1152	1783	-0.98	6.43	0.13
17L06-9-15	120	0.021150	0.000677	0.000641	0.000018	0.282433	0.000010	-12.00	-9.42	0.4	1147	1777	-0.98	6.48	0.27
DD17-1-O-01	124	0.017176	0.000187	0.000806	0.000009	0.282546	0.000013	-7.97	-5.28	0.5	993	1519	-0.98	6.09	0.24
DD17-1-O-02	124	0.036371	0.000550	0.001554	0.000018	0.282535	0.000015	-8.39	-5.82	0.5	1030	1551	-0.95	6.10	0.17
DD17-1-O-03	124	0.028492	0.000943	0.001238	0.000036	0.282499	0.000015	-9.66	-7.06	0.5	1072	1630	-0.96	6.02	0.22
DD17-1-O-04	124	0.028020	0.001670	0.001158	0.000066	0.282518	0.000014	-8.98	-6.36	0.5	1043	1586	-0.97	6.25	0.17
DD17-1-O-05	124	0.044011	0.000358	0.001818	0.000013	0.282510	0.000017	-9.27	-6.70	0.6	1073	1607	-0.95	6.37	0.18
DD17-1-O-06	124	0.037099	0.001102	0.001610	0.000043	0.282474	0.000018	-10.53	-7.94	0.6	1118	1686	-0.95	6.96	0.24
DD17-1-O-07	124	0.022249	0.000531	0.000946	0.000020	0.282469	0.000026	-10.70	-8.01	0.9	1105	1693	-0.97	6.42	0.21
DD17-1-O-08	124	0.048950	0.000469	0.001957	0.000011	0.282481	0.000028	-10.31	-7.71	1.0	1119	1673	-0.94	6.27	0.20
DD17-1-O-09	124	0.022487	0.000422	0.000984	0.000020	0.282496	0.000014	-9.75	-7.13	0.5	1068	1634	-0.97	6.06	0.16

DD17-1-O-10	124	0.041928	0.000298	0.001722	0.000007	0.282471	0.000021	-10.66	-8.02	0.7	1126	1693	-0.95	5.73	0.19
DD17-1-O-11	124	0.018821	0.000596	0.000822	0.000025	0.282513	0.000012	-9.16	-6.53	0.4	1040	1596	-0.98	6.14	0.18
DD17-1-O-12	124	0.041951	0.000610	0.001773	0.000024	0.282503	0.000016	-9.51	-6.93	0.5	1081	1622	-0.95	6.07	0.15
DD17-1-O-13	124	0.044219	0.000173	0.001828	0.000005	0.282492	0.000014	-9.90	-7.31	0.5	1099	1647	-0.94	6.39	0.12
DD17-1-O-14	124	0.009688	0.000406	0.000438	0.000017	0.282508	0.000012	-9.34	-6.68	0.4	1037	1606	-0.99	6.25	0.15
DD17-1-O-15	124	0.015553	0.000574	0.000709	0.000026	0.282503	0.000013	-9.51	-6.78	0.5	1051	1615	-0.98	6.42	0.20

Table S5. Major and trace element data of plagioclase.

Sample	16L05-1-01	16L05-1-02	16L05-1-03	16L05-1-04	16L05-1-05	16L05-1-06	17L02-1-01	17L02-1-02	17L02-1-03	17L02-1-04	17L02-1-05
Lithology	appinites						appinites				
Pluton	Qinggouzi						Dongshanzui				
SiO_2	54.42	56.82	55.97	54.76	53.40	53.89	55.76	55.40	55.01	58.60	58.22
TiO_2	2.86	2.53	2.27	2.39	2.66	2.43	0.02	0.00	0.00	0.00	0.07
Al_2O_3	28.35	26.82	27.43	27.99	29.01	28.72	27.87	28.26	28.64	25.84	25.93
FeO	0.28	0.21	0.20	0.22	0.26	0.23	0.13	0.09	0.09	0.08	0.14
MnO	0.00	0.00	0.00	0.01	0.00	0.01	0.00	0.00	0.00	0.00	0.00
MgO	0.02	0.02	0.01	0.02	0.02	0.01	0.00	0.00	0.00	0.00	0.01
CaO	11.08	9.09	9.61	10.53	11.75	11.28	9.64	9.73	10.03	7.83	8.29
Na_2O	5.34	6.58	6.30	5.44	5.00	5.41	6.13	6.07	5.80	7.24	6.95
K_2O	0.16	0.16	0.17	0.61	0.21	0.12	0.21	0.22	0.21	0.19	0.19
P_2O_5	0.04	0.03	0.04	0.04	0.03	0.03	0.01	0.03	0.02	0.01	0.01
Total	102.55	102.26	102.00	102.01	102.34	102.15	99.79	99.79	99.80	99.81	99.80
Sc	2.86	2.53	2.27	2.39	2.66	2.43	0.86	0.66	0.47	0.63	0.82
V	0.20	0.00	0.11	0.01	0.04	0.13	0.35	0.00	0.00	0.06	1.87
Cr	1.74	0.00	0.00	2.13	1.37	2.02	0.00	3.73	4.50	0.00	2.44
Co	0.12	0.11	0.09	1.14	0.12	6.80	0.03	0.26	0.08	0.04	0.53
Ni	0.92	0.23	1.84	0.24	0.00	3.36	1.41	0.00	0.16	0.00	0.30
Cu	0.73	0.50	3.17	0.63	0.21	3.64	0.43	1.70	1.31	0.41	2.97
Zn	3.70	3.42	3.77	3.11	3.82	3.04	1.19	2.16	1.50	2.04	2.32
Ga	23.34	21.20	23.49	24.41	23.25	24.10	27.38	25.04	26.54	24.89	26.98
Rb	0.77	0.48	0.91	4.03	1.00	0.45	0.03	0.71	1.43	0.07	0.65

Sr	2042	1718	1734	1887	2017	1883	1446	1473	1461	1383	1364
Y	0.10	0.07	0.08	0.11	0.10	0.15	0.31	0.12	0.02	0.02	0.09
Zr	0.02	0.02	0.02	0.00	0.15	0.05	0.08	0.07	0.00	0.00	0.14
Nb	0.00	0.01	0.00	0.00	0.00	0.01	0.13	0.00	0.00	0.00	0.22
Cs	0.05	0.05	0.00	0.00	0.00	0.00	0.01	0.30	0.02	0.00	0.01
Ba	410	458	337	1200	557	306	181	173	159	184	172
La	11.23	10.63	12.51	11.45	12.13	12.06	31.35	3.91	4.67	3.56	6.71
Ce	11.02	8.65	10.85	12.06	11.70	11.86	35.79	3.53	3.70	2.41	4.50
Pr	0.74	0.49	0.67	0.63	0.77	0.72	2.66	0.25	0.23	0.12	0.18
Nd	1.44	1.00	1.40	1.41	1.48	1.16	7.19	0.56	0.63	0.27	0.40
Sm	0.09	0.00	0.11	0.03	0.12	0.11	0.66	0.08	0.00	0.00	0.02
Eu	0.53	0.67	0.57	0.44	0.50	0.54	0.68	0.47	0.42	0.15	0.15
Gd	0.09	0.04	0.08	0.05	0.10	0.04	0.29	0.09	0.00	0.00	0.00
Tb	0.00	0.00	0.01	0.00	0.00	0.01	0.01	0.01	0.00	0.00	0.00
Dy	0.03	0.01	0.02	0.02	0.05	0.02	0.09	0.01	0.01	0.00	0.00
Ho	0.00	0.01	0.01	0.01	0.00	0.01	0.01	0.00	0.00	0.00	0.00
Er	0.00	0.00	0.01	0.01	0.00	0.02	0.00	0.03	0.00	0.00	0.03
Tm	0.00	0.00	0.00	0.00	0.00	0.00	0.00	0.00	0.00	0.00	0.00
Yb	0.00	0.01	0.02	0.01	0.01	0.03	0.00	0.01	0.00	0.00	0.01
Lu	0.00	0.00	0.01	0.00	0.00	0.01	0.00	0.00	0.00	0.00	0.01
Hf	0.00	0.00	0.00	0.00	0.01	0.00	0.02	0.01	0.00	0.00	0.02
Ta	0.00	0.00	0.00	0.00	0.00	0.00	0.00	0.00	0.00	0.00	0.00
Pb	7.92	10.93	11.13	10.13	8.89	12.65	15.64	15.94	15.22	17.37	17.10
Th	0.04	0.02	0.10	0.03	0.03	0.06	0.47	0.01	0.00	0.00	0.05
U	0.00	0.00	0.00	0.00	0.01	0.00	0.01	0.04	0.01	0.01	0.10

Table S6. In situ Pb isotopes of plagioclase.

Pluton and sample	Age(Ma)	$^{206}Pb/^{204}Pb$	2σ	$^{207}Pb/^{204}Pb$	2σ	$^{208}Pb/^{204}Pb$	2σ
Qinggouzi appinites							
16L05-1-01	125	18.304	0.030399	15.641	0.026786	39.026	0.066353
16L05-1-02	125	18.306	0.030741	15.665	0.029079	39.074	0.071352
16L05-1-03	125	18.349	0.028317	15.675	0.024174	39.091	0.057402
16L05-1-04	125	18.314	0.028244	15.682	0.026721	39.046	0.059889
16L05-1-05	125	18.324	0.029775	15.662	0.031119	39.079	0.064039
16L05-1-06	125	18.316	0.033295	15.659	0.029735	39.069	0.073396
Dongshanzui appinites							
17L02-1-01	121	15.990	0.027636	15.216	0.025162	39.833	0.060987
17L02-1-02	121	15.984	0.023069	15.211	0.021791	39.791	0.053516
17L02-1-03	121	16.020	0.024636	15.235	0.022963	39.772	0.057048
17L02-1-04	121	16.049	0.020525	15.229	0.018266	39.625	0.047579
17L02-1-05	121	16.059	0.018707	15.257	0.019567	39.757	0.052056
17L02-1-06	121	16.055	0.023946	15.253	0.022324	39.745	0.057620
17L02-1-07	121	16.110	0.027434	15.266	0.024391	39.756	0.064278
17L02-1-08	121	16.079	0.019949	15.272	0.017429	39.847	0.045613
17L02-1-09	121	16.100	0.019449	15.301	0.021592	39.844	0.052924
17L02-1-10	121	16.092	0.022905	15.299	0.021995	39.765	0.055622

Summary of cited references in main text Figures 1, 2, 4, 5, and 6.

REFERENCES (main text, Figure 1)

Azer, M.K., Gahlan, H.A., Asimow, P.D., and Alfaifi, H.J., 2018, Prehnite as an indicator mineral in the Wadi Nasb uralitized gabbro, South Sinai, Egypt: Journal of Asian Earth Sciences, v. 160, p. 107–117, https://doi.org/10.1016/j.jseaes.2018.04.011.

Azizi, H., Hadad, S., Stern, R.J., and Asahara, Y., 2019, Age, geochemistry, and emplacement of the ~40-Ma Baneh granite-appinite complex in a transpressional tectonic regime, Zagros suture zone, northwest Iran: International Geology Review, v. 61, p. 195–223, https://doi.org/10.1080/00206814.2017.1422394.

Barnes, C.G., Prestvik, T., Barnes, M.A.W., Anthony, E.Y., and Allen, C.M., 2003, Geology of a magma transfer zone: The Hortavær Igneous Complex, north-central Norway: Norsk Geologisk Tidsskrift, v. 83, p. 187–208.

Bea, F., Gallastegui, G., Montero, P., Molina, J.F., Scarrow, J., Cuestra, A., and González-Menéndez, L., 2021, Contrasting high-Mg, high-K rocks in Central Iberia: the appinite-vaugnerite conundrum and their (non-existent) relation with arc magmatism: Journal of Iberian Geology, v. 47, p. 235–261, https://doi.org/10.1007/s41513-020-00152-x.

Castro, A., Corretge, L.G., De la Rosa, J.D., Fernandez, C., Lopez, S., Garcia-Moreno, O., and Chacon, H., 2003, The appinite-migmatite complex of Sanabria, NW Iberian massif, Spain: Journal of Petrology, v. 44, p. 1309–1344, https://doi.org/10.1093/petrology/44.7.1309.

Chang, J., Audétat, A., and Li, J.W., 2021, In situ reaction-replacement origin of hornblendites in the Early Cretaceous Laiyuan complex, North China Craton, and implications for its tectono-magmatic evolution: Journal of Petrology, v. 62, p. 1–25, https://doi.org/10.1093/petrology/egab030.

Chew, D.M., and Stillman, C.J., 2009, Late Caledonian orogeny and magmatism, *in* Holland, C.H., and Sanders, I.S., eds., The Geology of Ireland, 2nd ed. Dunedin Academic Press, Edinburgh, pp. 143–173.

Corrales, F.F.P., Dussin, I.A., Heilbron, M., Bruno, H., Bersan, S., Valeriano, C.M., Pedrosa-Soares, A.C., and Tedeschi, M., 2020, Coeval high Ba-Sr arc-related and OIB Neoproterozoic rocks linking precollisional magmatism of the Ribeira and Araçuaí orogenic belts, SE-Brazil: Precambrian Research, v. 337, p. 105476, https://doi.org/10.1016/j.precamres.2019.105476.

Ding, L.X., Ma, C.Q., Li, J.W., and Wang, L.X., 2016, Geochronological, geochemical and mineralogical constraints on the petrogenesis of appinites from the Laoniushan complex, eastern Qinling, central China: Chemie der Erde, v. 76, p. 579–595, https://doi.org/10.1016/j.chemer.2016.10.002.

Domenick, M.A., and Basu, A.R., 1982, Age and origin of the Cortlandt Complex, New York: implications from Sm-Nd data: Contributions to Mineralogy and Petrology, v. 79, p. 290–294, https://doi.org/10.1007/BF00371520.

El-Rahman, Y.A., Seifert, T., Gutzmer, J., Said, A., Hofmann, M., Gärtner, A., and Linnemann, U., 2017, The South UmMongul Cu-Mo-Au prospect in the Eastern Desert of Egypt: From a mid-Cryogenian continental arc to Ediacaran post-collisional appinite-high Ba-Sr monzogranite: Ore Geology Reviews, v. 80, p. 250–266, https://doi.org/10.1016/j.oregeorev.2016.06.004.

Fan, W.B., Jiang, N., Xu, X.Y., Hu, J., and Zong, K.Q., 2017, Petrogenesis of the middle Jurassic appinite and coeval granitoids in the Eastern Hebei area of North China Craton: Lithos, v. 278–281, p. 331–346, https://doi.org/10.1016/j.lithos.2017.01.030.

Fazlnia, A., 2019, Petrogenesis and tectonic significance of Sardasht syenite-monzonite-gabbro-appinite intrusions, NW Iran: International Journal of Earth Sciences, v. 108, p. 49–66, https://doi.org/10.1007/s00531-018-1641-7.

Fortey, N.J., Cooper, A.H., Henney, P.J., Colman, T., and Nancarrow, P.H.A., 1994, Appinitic intrusions in the English Lake District: Mineralogy and Petrology, v. 51, p. 355–375, https://doi.org/10.1007/BF01159737.

Fowler, M.B., and Henney, P.J., 1996, Mixed Caledonian appinite magmas: implications for lamprophyre fractionation and high Ba-Sr granite genesis: Contributions to Mineralogy and Petrology, v. 126, p. 199–215, https://doi.org/10.1007/s004100050244.

Gahlan, H.A., Obeid, M.A., Azer, M.K., and Asimow, P.D., 2018, An example of post-collisional appinitic magmatism with an arc-like signature: the Wadi Nasb mafic intrusion, north Arabian-Nubian Shield, south Sinai, Egypt: International Geology Review, v. 60, p. 865–888, https://doi.org/10.1080/00206814.2017.1360804.

Huang, F., Zhang, Z., Xu, J.F., Li, X.Y., Zeng, Y.C., Wang, B.D., Li, X.W., Xu, R., Fan, Z.C., and Tian, Y., 2019, Fluid flux in the lithosphere beneath southern Tibet during Neo-Tethyan slab breakoff: Evidence from an appinite-granite suite: Lithos, v. 344–345, p. 324–338, https://doi.org/10.1016/j.lithos.2019.07.004.

Jarrar, G.H., Stern, R.J., Theye, T., Yaseen, N., Pease, V., Miller, N., Ibrahim, K.M., Passchier, C.W., and Whitehouse, M., 2017, Neoproterozoic Rosetta Gabbro from northernmost Arabian-Nubian Shield, south Jordan: Geochemistry and petrogenesis: Lithos, v. 284–285, p. 545–559, https://doi.org/10.1016/j.lithos.2017.05.008.

Leite, A.F.G.D., Fuck, R.E., Dantas, E.L., and Ruiz, A.S., 2021, Appinitic and high Ba-Sr magmatism in central Brazil: Insights into the late accretion stage of West Gondwana: Lithos, v. 398–399, p. 106333, https://doi.org/10.1016/j.lithos.2021.106333.

Ma, X., Chen, B., Chen, J.F., and Niu, X.L., 2013, Zircon SHRIMP U-Pb age, geochemical, Sr-Nd isotopic, and in-situ Hf isotopic data of the Late Carboniferous-Early Permian plutons in the northern margin of the North China Craton: Science China. Earth Sciences, v. 56, p. 126–144, https://doi.org/10.1007/s11430-012-4456-6.

Ma, X.X., Meert, J.G., Xu, Z.Q., and Yi, Z.Y., 2018, Late Triassic intra-oceanic arc system within Neotethys: Evidence from cumulate appinite in the Gangdese belt, southern Tibet: Lithosphere, v. 10, p. 545–565, https://doi.org/10.1130/L682.1.

Ma, Y.F., Liu, Y.J., Qin, T., Sun, W., Zhang, Y.Q., and Zhang, Y.J., 2020, Late Devonian to early Carboniferous magmatism in the western Songliao-Xilinhot block, Northeast China: Implications for eastward subduction of the Nenjiang oceanic lithosphere: Geological Journal, v. 55, p. 2208–2231, https://doi.org/10.1002/gj.3739.

Murphy, J.B., Hynes, A.J., and Cousens, B., 1997a. Tectonic influence on late Proterozoic Avalonian magmatism: an example from the Greendale Complex, Antigonish Highlands, Nova Scotia, Canada, *in* Sinha, A.K., Whalen, J.B., and Hogan, J.P., eds., The Nature of Magmatism in the Appalachian Orogen: Geological Survey of America Memoir, 191, p. 255–274, https://doi.org/10.1130/0-8137-1191-6.255.

Murphy, J.B., Keppie, J.D., Davis, D., and Krogh, T.E., 1997b, Regional significance of new U-Pb age data for Neoproterozoic igneous units in Avalonian rocks of northern mainland Nova Scotia, Canada: Geological Magazine, v. 134, p. 113–120, https://doi.org/10.1017/S0016756897006596.

Murphy, J.B., Nance, R.D., Gabler, L.B., Martell, A., and Archibald, D.A., 2019, Age, geochemistry and origin of the Ardara appinite plutons, Northwest Donegal, Ireland: Geoscience Canada, v. 46, p. 31–48, https://doi.org/10.12789/geocanj.2019.46.144.

Pe-Piper, G., Piper, D.J.W., and Tsikouras, B., 2010, The late Neoproterozoic Frog Lake hornblende gabbro pluton, Avalon Terrane of Nova Scotia: evidence for the origins of appinites: Canadian Journal of Earth Sciences, v. 47, p. 103–120, https://doi.org/10.1139/E09-077.

Pe-Piper, G., and Piper, D., 2018, The Jeffers Brook diorite-granodiorite pluton: style of emplacement and role of volatiles at various crustal levels in Avalonian appinites, Canadian Appalachians: International Journal of Earth Sciences, v. 107, p. 863–883, https://doi.org/10.1007/s00531-017-1536-z.

Richards, J.P., Chappell, B.W., and McCulloch, M.T., 1990, Intraplate-type magmatism in a continent-island-arc collision zone; Porgera intrusive complex, Papua New Guinea: Geology, v. 18, p. 958–961, https://doi.org/10.1130/0091-7613(1990)018<0958:ITMIAC>2.3.CO;2.

Rogers, G., and Dunning, G.R., 1991, Geochronology of appinitic and related granitic magmatism in the W highlands of Scotland: constraints on the timing of transcurrent fault movement: Journal of the Geological Society, v. 148, p. 17–27, https://doi.org/10.1144/gsjgs.148.1.0017.
Samson, S.D., and D'Lemos, R.S., 1999, A precise late Neoproterozoic U-Pb zircon age for the syntectonic Perelle quartz diorite, Guernsey, Channel Islands, UK: Journal of the Geological Society, v. 156, p. 47–54, https://doi.org/10.1144/gsjgs.156.1.0047.
Wang, Y.J., Fan, W.M., Zhang, H.F., and Peng, T.P., 2006, Early Cretaceous gabbroic rocks from the Taihang Mountains: Implications for a paleosubduction-related lithospheric mantle beneath the central North China Craton: Lithos, v. 86, p. 281–302, https://doi.org/10.1016/j.lithos.2005.07.001.
Wang, Z.Z., Han, B.F., Feng, L.X., and Liu, B., 2015, Geochronology, geochemistry and origins of the Paleozoic-Triassic plutons in the Langshan area, western Inner Mongolia, China: Journal of Asian Earth Sciences, v. 97, p. 337–351, https://doi.org/10.1016/j.jseaes.2014.08.005.
Wilkin, R.T., and Bornhorst, T.J., 1993, Archean Appinites from the Northern Complex, Michigan: The Journal of Geology, v. 101, p. 107–114, https://doi.org/10.1086/648199.
Wu, D.Q., Sun, F.Y., Pan, Z.C., and Tian, N., 2021, Geochronology, geochemistry, and Hf isotopic compositions of Triassic igneous rocks in the easternmost segment of the East Kunlun Orogenic Belt, NW China: implications for magmatism and tectonic evolution: International Geology Review, v. 63, p. 1011–1029, https://doi.org/10.1080/00206814.2020.1740895.
Xiong, F.H., Ma, C.Q., Wu, L., Jiang, H.A., and Liu, B., 2015, Geochemistry, zircon U-Pb ages and Sr-Nd-Hf isotopes of an Ordovician appinitic pluton in the East Kunlun orogen: New evidence for Proto-Tethyan subduction: Journal of Asian Earth Sciences, v. 111, p. 681–697, https://doi.org/10.1016/j.jseaes.2015.05.025.
Yang, D.G., Sun, D.Y., Gou, J., and Hou, X.G., 2017, Petrogenesis and tectonic setting of Carboniferous hornblende gabbros of the northern Great Xing'an Range, NE China: Constraints from geochronology, geochemistry, mineral chemistry, and zircon Hf isotopes: Geological Journal, v. 53, p. 2084–2098, https://doi.org/10.1002/gj.3035.
Ye, H.M., Li, X.H., Li, Z.X., and Zhang, C.L., 2008, Age and origin of high Ba-Sr appinite-granites at the northwestern margin of the Tibet Plateau: Implications for early Paleozoic tectonic evolution of the Western Kunlun orogenic belt: Gondwana Research, v. 13, p. 126–138, https://doi.org/10.1016/j.gr.2007.08.005.
Zhang, S.H., Zhao, Y., Liu, X.C., Liu, D.Y., Chen, F.K., Xie, L.W., and Chen, H.H., 2009, Late Paleozoic to Early Mesozoic mafic-ultramafic complexes from the northern North China Block: Constraints on the composition and evolution of the lithospheric mantle: Lithos, v. 110, p. 229–246, https://doi.org/10.1016/j.lithos.2009.01.008.
Zhang, X.H., Xue, F.H., Yuan, L.L., Ma, Y.G., and Wilde, S.A., 2012a, Late Permian appinite-granite complex from northwestern Liaoning, North China Craton: Petrogenesis and tectonic implications: Lithos, v. 155, p. 201–217, https://doi.org/10.1016/j.lithos.2012.09.002.
Zhang, X.H., Gao, Y.L., Wang, Z.J., Liu, H., and Ma, Y.G., 2012b, Carboniferous appinitic intrusions from the northern North China craton: geochemistry, petrogenesis and tectonic implications: Journal of the Geological Society, v. 169, p. 337–351, https://doi.org/10.1144/0016-76492011-062.
Zhang, X.H., Yuan, L.L., and Wilde, S.A., 2014, Crust/mantle interaction during the construction of an extensional magmatic dome: Middle to Late Jurassic plutonic complex from western Liaoning, North China Craton: Lithos, v. 205, p. 185–207, https://doi.org/10.1016/j.lithos.2014.07.006.
Zhang, B., Guo, F., Zhang, X.B., Wu, Y.M., Wang, G.Q., and Zhang, L., 2019, Early Cretaceous subduction of Paleo-Pacific Ocean in the coastal region of SE China: Petrological and geochemical constraints from the mafic intrusions: Lithos, v. 334–335, p. 8–24, https://doi.org/10.1016/j.lithos.2019.03.010.
Zhao, C., Qin, K.Z., Song, G.X., Li, G.M., and Mao, J.W., 2021a, The Triassic Duobaoshan appinite-granite suite, NE China: Implications for a water-fluxed lithosphericmantle and an extensional setting related to the subduction of the Mongol-Okhotsk Ocean: Lithos, v. 394–395, p. 106169, https://doi.org/10.1016/j.lithos.2021.106169.

Zhang, S.W., Yang, C., Lai, S.C., Pei, X.Z., Li, Z.C., and Zhu, R.Z., 2021b, Multistage fractional crystallization in the continental arc magmatic System: Constraints from the appinites in Tengchong Block, Southeastern extension of Tibet: Lithosphere, v. 1, p. 3367813.
Zhong, Y.F., Ma, C.Q., Liu, L., Zhao, J.H., Zheng, J.P., Nong, J.N., and Zhang, Z.J., 2014, Ordovician appinites in the Wugongshan Domain of the Cathaysia Block, South China: Geochronological and geochemical evidence for intrusion into a local extensional zone within an intracontinental regime: Lithos, v. 198–199, p. 202–216, https://doi.org/10.1016/j.lithos.2014.04.002.
Zhong, Y.F., Wang, L.X., Zhao, J.H., Liu, L., Ma, C.Q., Zheng, J.P., Zhang, Z.J., and Liu, B.J., 2016, Partial melting of an ancient sub-continental lithospheric mantle in the early Paleozoic intracontinental regime and its contribution to petrogenesis of the coeval peraluminous granites in South China: Lithos, v. 264, p. 224–238, https://doi.org/10.1016/j.lithos.2016.08.026.
Zhu, J., Li, Q.G., Chen, X., Tang, H.S., Wang, Z.Q., Chen, Y.J., Liu, S.W., Xiao, B., and Chen, J.L., 2018, Geochemistry and petrogenesis of the early Palaeozoic appinite-granite complex in the Western Kunlun Orogenic Belt, NW China: implications for Palaeozoic tectonic evolution: Geological Magazine, v. 155, p. 1641–1666, https://doi.org/10.1017/S0016756817000450.

REFERENCES (main text, Figure 2)

Kong, J.J., Niu, Y.L., Sun, P., Xiao, Y.Y., Guo, P.Y., Hong, D., Zhang, Y., Shao, F.L., Wang, X.H., and Duan, M., 2019, The origin and geodynamic significance of the Mesozoic dykes in eastern continental China: Lithos, v. 332–333, p. 328–339, https://doi.org/10.1016/j.lithos.2019.02.024.
Li, J.Y., Qian, Y., Sun, J.L., Li, H.R., Zhao, C.J., Sun, F.Y., and Shen, Y.J., 2021, Early Cretaceous granitoids and gabbro in the Liaodong Peninsula: implications for delamination of the North China Craton and Paleo-Pacific Plate subduction: Mineralogy and Petrology, v. 115, p. 299–322, https://doi.org/10.1007/s00710-020-00735-7.
Li, X.S., 2019, The petrogenesis and tectonic setting of the Early Cretaceous basic dikes in Pulandian area, Liaodong Peninsula [M.S. thesis]: Beijing, China University of Geosciences, 63 p. [in Chinese with English abstract].
Liu, J.X., Guo, W., and Zhu, K., 2016, Geochronology, geochemistry and geological significance of the Early Cretaceous intrusive rocks from Xiuyan area, eastern Liaodong Province [in Chinese with English abstract]: Yanshi Xuebao, v. 32, p. 2889–2990.
Liu, Y., Wei, J.H., Zhang, D.H., Chen, J.J., and Zhang, X.M., 2020, Early Cretaceous Wulong intermediate-mafic dike swarms in the Liaodong Peninsula: Implications for rapid lithospheric delamination of the North China Craton: Lithos, v. 362–363, p. 105473, https://doi.org/10.1016/j.lithos.2020.105473.
Ma, Q., Xu, Y.G., Zheng, J.P., Griffin, W.L., Hong, L.B., and Ma, L., 2016, Coexisting Early Cretaceous high-Mg andesites and adakitic rocks in the North China Craton: the role of water in intraplate magmatism and cratonic destruction: Journal of Petrology, v. 57, p. 1279–1308, https://doi.org/10.1093/petrology/egw040.
Miao, L.C., Zhang, F.Q., Liu, D.Y., Shi, Y.R., and Xie, H.Q., 2010, Zircon SHRIMP U-Pb dating for gabbro at Chaotiehe in the Haicheng area, eastern Liaoning: Chinese Science Bulletin, v. 55, p. 403–410, https://doi.org/10.1007/s11434-009-0404-z.
Pei, F.P., Xu, W.L., Yang, D.B., Yu, Y., Wang, W., and Zhao, Q.G., 2011, Geochronology and geochemistry of Mesozoic mafic-ultramafic complexes in the southern Liaoning and southern Jilin provinces, NE China: Constraints on the spatial extent of destruction of the North China Craton: Journal of Asian Earth Sciences, v. 40, p. 636–650, https://doi.org/10.1016/j.jseaes.2010.10.015.
Tan, J., Wei, J.H., Shi, W.J., Wang, M.Z., Li, Y.J., Fu, L.B., and Li, H., 2013, Formation of Wulong mafic dikes via mixing of enriched lithospheric mantle-derived and crustal magmas, eastern North China Craton: The Journal of Geology, v. 121, p. 517–535, https://doi.org/10.1086/671393.

REFERENCES (main text, Figure 4)

Fan, W.B., Jiang, N., Xu, X.Y., Hu, J., and Zong, K.Q., 2017, Petrogenesis of the middle Jurassic appinite and coeval granitoids in the Eastern Hebei area of North China Craton: Lithos, v. 278–281, p. 331–346, https://doi.org/10.1016/j.lithos.2017.01.030.

Huang, F., Zhang, Z., Xu, J.F., Li, X.Y., Zeng, Y.C., Wang, B.D., Li, X.W., Xu, R., Fan, Z.C., and Tian, Y., 2019, Fluid flux in the lithosphere beneath southern Tibet during Neo-Tethyan slab breakoff: Evidence from an appinite-granite suite: Lithos, v. 344–345, p. 324–338, https://doi.org/10.1016/j.lithos.2019.07.004.

Jing, W.C., 2017, Discovery of hornblende gabbro in Sangueda, Zetang, Tibet: Evidence of closure time of the Yarlung Zangbo. MD thesis of China University of Geosciences (Beijing) (65 p. (in Chinese with English abstract)).

Pei, F.P., Xu, W.L., Yang, D.B., Yu, Y., Wang, W., and Zhao, Q.G., 2011, Geochronology and geochemistry of Mesozoic mafic-ultramafic complexes in the southern Liaoning and southern Jilin provinces, NE China: Constraints on the spatial extent of destruction of the North China Craton: Journal of Asian Earth Sciences, v. 40, p. 636–650, https://doi.org/10.1016/j.jseaes.2010.10.015.

Sun, Y., 2016, Petrogenesis and Mineralization of the Early Cretaceous intrusive rocks in Handan-Xintai area, Hebei Province, China [Ph.D. thesis]: Wuhan, China University of Geosciences, 150 p. [in Chinese with English abstract].

Xin, W., Sun, F.Y., Zhang, Y.T., Fan, X.Z., Wang, Y.C., and Li, L., 2019, Mafic-intermediate igneous rocks in the East Kunlun Orogenic Belt, northwestern China: Petrogenesis and implications for regional geodynamic evolution during the Triassic: Lithos, v. 346–347, p. 105159, https://doi.org/10.1016/j.lithos.2019.105159.

Zhang, X.H., Xue, F.H., Yuan, L.L., Ma, Y.G., and Wilde, S.A., 2012a, Late Permian appinite-granite complex from northwestern Liaoning, North China Craton: Petrogenesis and tectonic implications: Lithos, v. 155, p. 201–217, https://doi.org/10.1016/j.lithos.2012.09.002.

Zhang, X.H., Gao, Y.L., Wang, Z.J., Liu, H., and Ma, Y.G., 2012b, Carboniferous appinitic intrusions from the northern North China craton: geochemistry, petrogenesis and tectonic implications: Journal of the Geological Society, v. 169, p. 337–351, https://doi.org/10.1144/0016-76492011-062.

Zhao, X., Fu, L.B., Wei, J.H., Zhao, Y.J., Tang, Y., Yang, B.R., Guan, B., and Wang, X.Y., 2017, Geological Characteristics of An'nage Hornblende Gabbro form East Kunlun Orogenic Belt and Its Constrains on Evolution of Paleo-Tethys Ocean [in Chinese with English abstract]: Earth Science, v. 43, p. 354–370.

Zhong, Y.F., Ma, C.Q., Liu, L., Zhao, J.H., Zheng, J.P., Nong, J.N., and Zhang, Z.J., 2014, Ordovician appinites in the Wugongshan Domain of the Cathaysia Block, South China: Geochronological and geochemical evidence for intrusion into a local extensional zone within an intracontinental regime: Lithos, v. 198–199, p. 202–216, https://doi.org/10.1016/j.lithos.2014.04.002.

Zhong, Y.F., Wang, L.X., Zhao, J.H., Liu, L., Ma, C.Q., Zheng, J.P., Zhang, Z.J., and Liu, B.J., 2016, Partial melting of an ancient sub-continental lithospheric mantle in the early Paleozoic intracontinental regime and its contribution to petrogenesis of the coeval peraluminous granites in South China: Lithos, v. 264, p. 224–238, https://doi.org/10.1016/j.lithos.2016.08.026.

Xiong, F.H., Ma, C.Q., Wu, L., Jiang, H.A., and Liu, B., 2015, Geochemistry, zircon U-Pb ages and Sr-Nd-Hf isotopes of an Ordovician appinitic pluton in the East Kunlun orogen: New evidence for Proto-Tethyan subduction: Journal of Asian Earth Sciences, v. 111, p. 681–697, https://doi.org/10.1016/j.jseaes.2015.05.025.

Liu, B., Ma, C.Q., Huang, J., Wang, L.X., Zhao, S.Q., Yan, R., Sun, Y., and Xiong, F.H., 2017, Petrogenesis and tectonic implications of Upper Triassic appinite dykes in the East Kunlun orogenic belt, northern Tibetan Plateau: Lithos, v. 284–285, p. 766–778, https://doi.org/10.1016/j.lithos.2017.05.016.

Tian, J., Teng, X.J., Liu, Y., Teng, F., He, P., Guo, S., Wang, W.L., 2018, Petrogenesis and tectonic significance of the Early Carboniferous hornblende gabbro and granodiorite in Langshan area, Inner Mongolia. Acta petrologica et mineralogical 37, 754–770 (in Chinese with English abstract).

REFERENCES (main text, Figure 5)

Deng, J., Liu, X.F., Wang, Q.F., Dilek, Y., and Liang, Y.Y., 2017, Isotopic characterization and petrogenetic modeling of Early Cretaceous mafic diking-Lithospheric extension in the North China craton, eastern Asia: Geological Society of America Bulletin, v. 129, p. 1379–1407, https://doi.org/10.1130/B31609.1.

Gu, Y.C., 2019, The Mesozoic tectonic-magmatic constraints on the gold mineralization in Wulong gold Mining Area, Eastern Liaoning [Ph.D. thesis]: Beijing, China University of Geosciences, 167 p. [in Chinese with English abstract].

Guo, F., Fan, W.M., Wang, Y.J., and Zhang, M., 2004, Origin of early Cretaceous calc-alkaline lamprophyres from the Sulu orogen in eastern China: implications for enrichment processes beneath continental collisional belt: Lithos, v. 78, p. 291–305, https://doi.org/10.1016/j.lithos.2004.05.001.

Kong, J.J., Niu, Y.L., Sun, P., Xiao, Y.Y., Guo, P.Y., Hong, D., Zhang, Y., Shao, F.L., Wang, X.H., and Duan, M., 2019, The origin and geodynamic significance of the Mesozoic dykes in eastern continental China: Lithos, v. 332–333, p. 328–339, https://doi.org/10.1016/j.lithos.2019.02.024.

Li, S.Z., Liu, J.Z., Zhao, G.C., Wu, F.Y., Han, Z.Z., and Yang, Z.Z., 2004, Key geochronology of Mesozoic deformation in the eastern block of the North China Craton and its constraints on regional tectonics: A case of Jiaodong and Liaodong Peninsula [in Chinese with English Abstract]: Yanshi Xuebao, v. 20, p. 633–646.

Li, X.S., 2019, The petrogenesis and tectonic setting of the Early Cretaceous basic dikes in Pulandian area, Liaodong Peninsula [M.S. thesis]: Beijing, China University of Geosciences, 63 p. [in Chinese with English abstract].

Li, X.Y., Li, S., Suo, Y., Somerville, I.D., Huang, F., Liu, X., Wang, P., Han, Z., and Jin, L., 2018, Early Cretaceous diabases, lamprophyres and andesites-dacites in western Shandong, North China Craton: Implications for local delamination and Paleo-Pacific slab rollback: Journal of Asian Earth Sciences, v. 160, p. 426–444, https://doi.org/10.1016/j.jseaes.2017.08.005.

Liu, Y., Wei, J.H., Zhang, D.H., Chen, J.J., and Zhang, X.M., 2020, Early Cretaceous Wulong intermediate-mafic dike swarms in the Liaodong Peninsula: Implications for rapid lithospheric delamination of the North China Craton: Lithos, v. 362–363, p. 105473, https://doi.org/10.1016/j.lithos.2020.105473.

Ma, L., Jiang, S.Y., Hofmann, A.W., Dai, B.Z., Hou, M.L., Zhao, K.D., Chen, L.H., Li, J.W., and Jiang, Y.H., 2014a, Lithospheric and asthenospheric sources of lamprophyres in the Jiaodong Peninsula: a consequence of rapid lithospheric thinning beneath the North China Craton?: Geochimica et Cosmochimica Acta, v. 124, p. 250–271, https://doi.org/10.1016/j.gca.2013.09.035.

Ma, L., Jiang, S.Y., Hofmann, A.W., Xu, Y.G., Dai, B.Z., and Hou, M.L., 2016, Rapid lithospheric thinning of the North China Craton: New evidence from cretaceous mafic dikes in the Jiaodong Peninsula: Chemical Geology, v. 432, p. 1–15, https://doi.org/10.1016/j.chemgeo.2016.03.027.

Ma, L., Jiang, S.Y., Hou, M.L., Dai, B.Z., Jiang, Y.H., Yang, T., Zhao, K.D., Pu, W., Zhu, Z.Y., and Xu, B., 2014b, Geochemistry of Early Cretaceous calc-alkaline lamprophyres in the Jiaodong Peninsula: Implication for lithospheric evolution of the eastern North China Craton: Gondwana Research, v. 25, p. 859–872, https://doi.org/10.1016/j.gr.2013.05.012.

Pang, C.J., Wang, X.C., Xu, Y.G., Wen, S.N., Kuang, W.S., and Hong, L.B., 2015, Pyroxenite-derived Early Cretaceous lavas in the Liaodong Peninsula: Implication for metasomatism and thinning of the lithospheric mantle beneath North China Craton: Lithos, v. 227, p. 77–93, https://doi.org/10.1016/j.lithos.2015.03.022.

Pei, F.P., Xu, W.L., Yang, D.B., Yu, Y., Wang, W., and Zhao, Q.G., 2011, Geochronology and geochemistry of Mesozoic mafic-ultramafic complexes in the southern Liaoning and southern Jilin

provinces, NE China: Constraints on the spatial extent of destruction of the North China Craton: Journal of Asian Earth Sciences, v. 40, p. 636–650, https://doi.org/10.1016/j.jseaes.2010.10.015.
Tan, J., Wei, J.H., Shi, W.J., Wang, M.Z., Li, Y.J., Fu, L.B., and Li, H., 2013, Formation of Wulong mafic dikes via mixing of enriched lithospheric mantle-derived and crustal magmas, Eastern North China Craton: The Journal of Geology, v. 121, p. 517–535, https://doi.org/10.1086/671393.
Wu, F.Y., Yang, J.H., Wilde, S.A., and Zhang, X.O., 2005b, Geochronology, petrogenesis and tectonic implications of Jurassic granites in the Liaodong Peninsula, NE China: Chemical Geology, v. 221, p. 127–156, https://doi.org/10.1016/j.chemgeo.2005.04.010.
Yang, J.H., Wu, F.Y., Chung, S.L., Wilde, S.A., and Chu, M.F., 2006, A hybrid origin for the Qianshan A-type granite, northeast China: Geochemical and Sr-Nd-Hf isotopic evidence: Lithos, v. 89, p. 89–106, https://doi.org/10.1016/j.lithos.2005.10.002.
Zhang, H.F., Sun, M., Zhou, X.H., Fan, W.M., Zhai, M.G., and Yin, J.F., 2002, Mesozoic lithosphere destruction beneath the North China Craton:evidence from major-,trace-element and Sr-Nd-Pb isotope studies of Fangcheng basalts: Institute of Geology and Geophysics, Chinese academy of sciences (Compilation of Academic Abstracts), p. 241–254.

REFERENCES (main text, Figure 6)

Gu, Y.C., Chen, R.Y., Li, D.T., Yang, J.L., Yang, F.C., Jia, H.X., Dick, J., Hu, Q.H., Ju, N., and Cao, J., 2017, Jurassic ca. 160 Ma crustal remelting and Paleoproterozoic intrusive rock residues in the Liaodong Peninsula, East China: Evidence from in situ zircon U-Pb dating and Lu-Hf isotopic analysis: Geological Journal, v. 53, p. 174–188, https://doi.org/10.1002/gj.3206.
Gu, Y.C., 2019, The Mesozoic tectonic-magmatic constraints on the gold mineralization in Wulong gold Mining Area, Eastern Liaoning [Ph.D. thesis]: Beijing, China University of Geosciences, 167 p. [in Chinese with English abstract].
Sun, J.F., Zhang, J.H., Yang, J.H., Zhu, Y.S., Chen, J.Y., and Ling-Hu, M.M., 2020, Multi-stage Jurassic magmatism in the Liaodong Peninsula: Constraints on crustal evolution beneath the eastern North China Craton: Lithos, v. 334–335, p. 42–57.
Xue, J.X., Liu, Z.H., Liu, J.X., Dong, X.J., Feng, F., and Lian, G.H., 2020, Geochemistry, Geochronology, Hf Isotope and Tectonic Significance of Late Jurassic Huangdi Pluton in Xiuyan, Liaodong Peninsula: Earth Science, v. 45, p. 2030–2043 [in Chinese with English abstract].
Zhang, Z.C., Wang, Y.W., Li, D.D., and Lai, C., 2019, Lithospheric Architecture and Metallogenesis in Liaodong Peninsula, North China Craton: Insights from Zircon Hf-Nd Isotope Mapping: Minerals (Basel), v. 9, no. 3, https://doi.org/10.3390/min9030179.